Available online at www.sciencedirect.com
SCIENCE DIRECT®
ELSEVIER
Physica D xxx (2003) xxx–xxx
PHYSICA D
www.elsevier.com/locate/physd

Spatially periodic modulation of cortical patterns by long-range horizontal connections

Paul C. Bressloff*

Department of Mathematics, University of Utah, Salt Lake City, UT 84112, USA

Received 10 June 2003; received in revised form 10 June 2003; accepted 29 June 2003
Communicated by J.P. Keener

Abstract

We analyze spontaneous pattern formation in a continuum model of primary visual cortex that incorporates spatially periodic inhomogeneities in the distribution of long-range horizontal connections. These inhomogeneities reflect the underlying crystalline-like structure of cortex, as exemplified by the distribution of cytochrome oxidase blobs. We first solve the linear eigenvalue problem for a primary Turing instability, and show how the resulting activity pattern can lock to the underlying cortical lattice when certain resonance conditions are satisfied. This result is then extended to the weakly nonlinear regime by performing a multiple scale perturbation expansion of the nonlocal integro-differential equation that determines cortical activity. The resulting amplitude equation describes the effects of long-wavelength modulations of a primary roll pattern in the presence of periodic inhomogeneities, and is shown to exhibit a commensurate–incommensurate transition analogous to that found in convective fluid systems with external periodic forcing. Extensions of our theory to models of cortical development are briefly discussed.

PACS: 87.19.La/sep 05.45.-a

Keywords: Neural pattern formation; Visual cortex

1. Introduction

One of the major simplifying assumptions in most large-scale models of cortical tissue is that the interactions between cell populations are homogeneous and isotropic, that is, that they are invariant under the action of the Euclidean group of rigid body motions in the plane. Euclidean symmetry plays a key role in determining the types of activity patterns that can be generated spontaneously in these cortical networks [12,21]. For example, it is well known that a homogeneous network can undergo a Turing-like instability due to competition between short-range excitation and longer-range inhibition [19,48]. Moreover, amplitude equations can be derived to investigate the selection and stability of these patterns close to the primary instability, with the basic structure of these equations determined by the underlying symmetries [8,9,16,19,20].

* Tel.: +1-801-585-1633; fax: +1-801-581-4148.
E-mail address: bressloff@math.utah.edu (P.C. Bressloff).

0167-2789/$ – see front matter © 2003 Published by Elsevier B.V.
doi:10.1016/S0167-2789(03)00238-0

However, the assumptions of homogeneity and isotropy are no longer valid when the detailed microstructure of cortex is taken into account. In fact, cortex has a distinctly crystalline-like structure at the millimeter length-scale [26]. This is exemplified by the distribution of cytochrome oxidase (CO) blobs found in the primary visual cortex (V1) of cats and primates. These regions, which are about 0.2 mm in diameter and about 0.6 mm apart, coincide with cells that are more metabolically active in response to visual stimuli, and hence richer in their levels of CO [25]. Moreover, the distribution of the CO blobs is correlated with a number of periodically repeating feature maps in which local populations of neurons respond preferentially to stimuli with particular properties such as orientation, spatial frequency and left/right eye (ocular) dominance [36,43]. It has thus been suggested that the CO blobs are the sites of functionally and anatomically distinct channels of visual processing [28,41]. Another manifestation of the crystalline-like structure of cortex is the distribution of singularities or so-called pinwheels in the orientation preference map, where the scatter or rate of change of differing orientation preference label is much higher, so that there is a weakening of orientation selectivity at the population level. Away from the pinwheels there exist approximate linear zones within which iso-orientation regions form parallel slabs. The linear zones tend to cross the borders of ocular dominance stripes at right angles, whereas the pinwheels tend to align with the centers of ocular dominance stripes. CO blobs are also located in the centers of ocular dominance stripes and have a strong association with about half of the orientation singularities. All of these features can be seen in Fig. 1.

The periodic structure of visual cortex is reflected anatomically by the horizontally spreading connectional fields made by pyramidal neurons in the superficial layers of V1 (see Fig. 2). By matching anatomical projections with optically imaged feature maps, it has been shown that these horizontal connections, which extend several millimeters in cortex and are broken into discrete patches with a very regular size and spacing [23,24,38], tend to link neurons having common functional properties as determined, for example, by their proximity to CO blobs [7,31,49,50]. The patchy nature of the horizontal connections immediately implies breaking of continuous rotation symmetry but not necessarily continuous translation symmetry. For it is possible that the horizontal connections are still homogeneous, depending only on the relative location of two points in cortex. However, there is growing evidence that there exist inhomogeneities that break continuous translation symmetry as well. For example, an interesting recent experimental finding is that some cells located within intermediate distances from CO blobs have very little in the way of horizontal connections [50], thus leading to an effective reduction in connectivity at the population level. This suggests that there is a spatially periodic variation in the overall strength or range of the horizontal connections that is correlated with the location of CO blobs. Another possible source of periodic inhomogeneity arises from the anisotropy in the patchy connectional field as seen in Fig. 2. In some animals the direction of anisotropy is

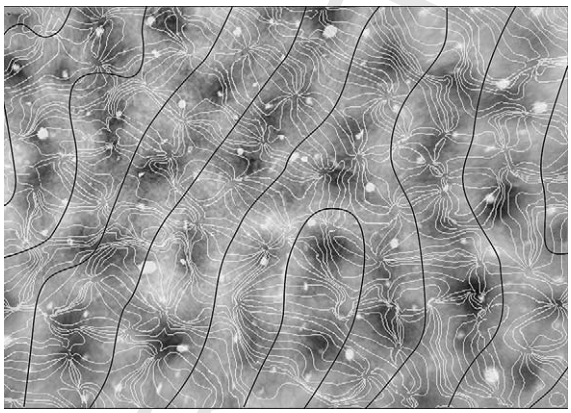

Fig. 1. Map of iso-orientation contours (light gray lines), ocular dominance boundaries (dark gray lines) and CO blob regions (shaded areas) of macaque V1. Redrawn from [5].

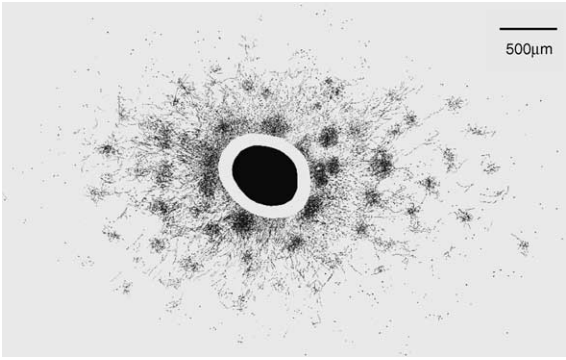

Fig. 2. Reconstruction of a tangential section through layers 2/3 of macaque area V1, showing a CTB injection site and surrounding transported orthograde and retrograde label. Redrawn from [30].

correlated with the orientation preference map and thus rotates periodically across cortex [7]. Although the visual cortex is the most studied region of the brain, there is growing evidence that analogous periodic structures appear in other cortical areas such as the rat barrel cortex [2] and auditory cortex [37]. A particularly striking example is found in the prefrontal cortex [27,32]. Here pyramidal cells in superficial layers are segregated into stripes that are mutually connected via horizontally projecting axon collaterals, whereas neurons within the gaps between stripes do not have horizontal connections. The functional role of these stripes is currently unknown.

In this paper we investigate how a spatially periodic inhomogeneity in the distribution of horizontal connections affects spontaneous pattern formation in a large-scale dynamical model of visual cortex. We treat the synaptic interactions mediated by the horizontal connections as an excitatory perturbation that generates a state-dependent, periodic forcing of an underlying homogeneous network. Under the assumption that the homogeneous network is close to a primary pattern forming instability, we use the method of multiple spatial and temporal scales to derive a form of Ginzburg–Landau amplitude equation. Our derivation explicitly takes into account the nonlocal nature of the neuronal interactions. The resulting amplitude equation describes the effects of long-wavelength modulations of a primary roll pattern and their coupling to the periodic forcing mediated by the horizontal connections. Following previous work on periodically forced convective systems [29,15,46], we show that when the wavelength of the primary pattern is commensurate with the periodic modulation of the horizontal connections, the spontaneous activity patterns lock to the cortical lattice. That is, the activity patterns explicitly reflect the crystalline-like structure of cortex.

The paper is organized along the following lines. Our cortical model of horizontal connections is introduced in Section 2 and the linear eigenvalue problem for pattern formation in the presence of periodic inhomogeneities is presented in Section 3. The detailed derivation of the amplitude equation for a one-dimensional roll pattern based on the method of multiple scales is presented in Section 4, followed by an analysis of long-wavelength instabilities and commensurate–incommensurate transitions in Section 5. Finally, in Section 6 we briefly discuss possible applications of our results to cortical development.

2. Cortical model with long-range horizontal connections

We model a layer of visual cortex as a continuous two-dimensional neural medium evolving according to the rate equation [11,21,47,48]

$$\tau \frac{\partial a(\mathbf{r}, t)}{\partial t} = -a(\mathbf{r}, t) + \int_{\mathbf{R}^2} w(\mathbf{r}|\mathbf{r}')\, f(a(\mathbf{r}', t))\, \mathrm{d}\mathbf{r}' + h_0. \tag{2.1}$$

Table 1
Generators for the planar lattices and their dual lattices

Lattice	ℓ_1	ℓ_2	$\hat{\ell}_1$	$\hat{\ell}_2$
Square	$(1, 0)$	$(0, 1)$	$(1, 0)$	$(0, 1)$
Hexagonal	$(1, 0)$	$\frac{1}{2}\left(1, \sqrt{3}\right)$	$\left(1, \frac{-1}{\sqrt{3}}\right)$	$\left(0, \frac{2}{\sqrt{3}}\right)$
Rhombic	$(1, 0)$	$(\cos\eta, \sin\eta)$	$(1, -\cot\eta)$	$(0, \csc\eta)$

The scalar field $a(\mathbf{r}, t)$ represents the local activity of a population of excitatory and inhibitory neurons at cortical position $\mathbf{r} = (x, y) \in \mathbf{R}^2$ at time t, τ is a membrane or synaptic time constant, h_0 is a uniform external input, and the distribution $w(\mathbf{r}|\mathbf{r}')$ is the strength of connections from neurons at $\mathbf{r}'$ to neurons at $\mathbf{r}$. In the following we fix the units of time by setting $\tau = 1$. The nonlinear firing-rate function f is assumed to be a smooth monotonically increasing function of the form

$$f(a) = \frac{1}{1 + \mathrm{e}^{-\gamma(a-\zeta)}} \tag{2.2}$$

for constant gain γ and threshold ζ. Motivated by the anatomy highlighted in Section 1, we decompose the weight distribution w according to

$$w(\mathbf{r}|\mathbf{r}') = W_0(|\mathbf{r} - \mathbf{r}'|) + \kappa w_{\mathrm{hoz}}(\mathbf{r}|\mathbf{r}'), \tag{2.3}$$

where W_0 represents isotropic and homogeneous local connections that depend on the Euclidean distance $|\mathbf{r} - \mathbf{r}'| = \sqrt{(x - x')^2 + (y - y')^2}$, w_{hoz} represents the distribution of excitatory horizontal connections and κ is a positive coupling parameter. Experimentally it is found that the horizontal connections modulate rather than drive a neuron's response to a visual stimulus [22,24,44], suggesting that κ is small.

In order to construct the distribution of long-range horizontal connections w_{hoz}, we first have to take into account the "patchiness" of these connections. Suppose that there exists a set of feature preferences $\mathcal{F}(\mathbf{r})$ (such as ocular dominance, orientation and spatial frequency) that varies periodically with respect to a regular planar lattice $\mathcal{L}_0$:

$$\mathcal{L}_0 = \{(m_1\ell_1 + m_2\ell_2)d_0 : m_1, m_2 \in \mathbf{Z}\}, \tag{2.4}$$

where ℓ_1 and ℓ_2 are the generators of the lattice and d_0 is the lattice spacing, which is taken to be of the order 1 mm. Let θ be the angle between the two basis vectors ℓ_1 and ℓ_2. We can then distinguish three types of lattice according to the value of θ: square lattice ($\theta = \pi/2$), rhombic lattice ($0 < \theta < \pi/2, \theta \neq \pi/3$) and hexagonal ($\theta = \pi/3$). After rotation, the generators of the planar lattices are given in Table 1. Also shown are the generators of the *dual lattice* $\hat{\mathcal{L}}_0$ satisfying $\hat{\ell}_i \cdot \ell_j = \delta_{i,j}$. Given the lattice $\mathcal{L}_0$, we can partition the cortex into a set of fundamental domains, each of which corresponds to a so-called functional *hypercolumn* [36]. A hypercolumn is defined to be a region approximately 1 mm^2 in surface area that contains two orientation pinwheels and one CO blob per ocular dominance column. The local connections span a single hypercolumn, whereas the patchy horizontal connections link cells with similar feature preferences in distinct hypercolumns.[1] We implement the latter condition by introducing the doubly periodic feature map $\mathcal{P}(\mathbf{r})$

$$\mathcal{P}(\mathbf{r}) = \frac{1}{2}\sum_{i=1}^{2} \cos\left(\frac{2\pi\mathbf{r}\cdot\hat{\ell}_i}{d_0}\right), \tag{2.5}$$

[1] Elsewhere we have developed an alternative model of visual cortex based on a lattice of coupled hypercolumns [11]. In this model cortical position $\mathbf{r}$ is replaced by the set $\{\ell, \mathcal{F}\}$ with $\ell \in \mathcal{L}_0$ labeling a particular hypercolumn and $\mathcal{F}$ labeling the feature preferences of neurons at a particular point within the hypercolumn. The associated weight distribution is decomposed into local and long-range parts according to $w(\ell, \mathcal{F}|\ell', \mathcal{F}') = W_0(\mathcal{F}|\mathcal{F}')\delta_{\ell,\ell'} + \kappa w_{\mathrm{hoz}}(\ell|\ell')\delta(\mathcal{F} - \mathcal{F}')$.

such that $-1 \leq \mathcal{P}(\mathbf{r}) \leq 1$ and $\mathcal{P}(\mathbf{r}+\ell) = \mathcal{P}(\mathbf{r})$ for all $\ell \in \mathcal{L}_0$. One can interpret $\mathcal{P}(\mathbf{r})$ as an index function that indicates the relative position of $\mathbf{r}$ with respect to the lattice $\mathcal{L}$. In particular, if $\mathcal{P}(\mathbf{r}) = \mathcal{P}(\mathbf{r}')$ then the neurons at $\mathbf{r}$ and $\mathbf{r}'$ have the same set of feature preferences.

Assuming for the moment that the horizontal connections are homogeneous, we set

$$w_{\rm hoz}(\mathbf{r}|\mathbf{r}') = \Theta(\mathcal{P}(\mathbf{r}-\mathbf{r}') - \mathcal{P}_0)\Theta(|\mathbf{r}-\mathbf{r}'| - d_0) J_0(|\mathbf{r}-\mathbf{r}'|) \equiv J(\mathbf{r}-\mathbf{r}'), \tag{2.6}$$

where Θ denotes the Heaviside step function. Here $\mathcal{P}_0$, $0 < \mathcal{P}_0 < 1$, is a threshold that fixes the size of the patches, and J_0 determines the variation in the strength of the connections with cortical separation. If $\mathcal{P}(\mathbf{r}-\mathbf{r}') < P_0$ then the cells at $\mathbf{r}$ and $\mathbf{r}'$ differ sufficiently in their given feature preferences so that $w_{\rm hoz}(\mathbf{r}|\mathbf{r}') = 0$, which means that the cells at $\mathbf{r}$ and $\mathbf{r}'$ are not linked. Also note that the first cortical patch occurs at a minimum cortical separation d_0. For concreteness, we assume that J_0 decreases exponentially with cortical separation:

$$J_0(|\mathbf{r}|) = K\,\mathrm{e}^{-|\mathbf{r}|/\xi} \tag{2.7}$$

with $\xi > d_0$. It follows from Eq. (2.6) that the total weight distribution (2.3) is translation invariant, since $w(\mathbf{r}+\mathbf{s}|\mathbf{r}'+\mathbf{s}) = w(\mathbf{r}|\mathbf{r}')$ for all $\mathbf{s} \in \mathbf{R}^2$, but it is not rotation invariant due to the discrete rotation symmetry of the lattice $\mathcal{L}_0$. Consider, for example, a square lattice $\mathcal{L}_0$ for which $\mathcal{P}(\mathbf{r}) = [\cos(2\pi x/d_0) + \cos(2\pi y/d_0)]/2$. In Fig. 3(a) we present a two-dimensional contour plot of $J(\Delta\mathbf{r})$ as a function of cortical separation $\Delta\mathbf{r} = \mathbf{r}-\mathbf{r}'$, which shows the distribution of patchy connections. A corresponding cross-section of J along the x-axis is shown in Fig. 3(b), together with an example of a local distribution W_0.

As we have highlighted in Section 1, there are a number of possible sources for a spatially periodic variation in the pattern of patchy connections as the location of the center of the distribution is shifted in the cortical plane. Eq. (2.6) will then have the more general form

$$w_{\rm hoz}(\mathbf{r}|\mathbf{r}') = \Theta(\mathcal{P}(\mathbf{r}-\mathbf{r}') - \mathcal{P}_0)\Theta(|\mathbf{r}-\mathbf{r}'| - d_0) J_0(\mathbf{r}|\mathbf{r}'), \tag{2.8}$$

where J_0 now includes the effects of periodic modulations. In order to motivate the detailed structure of J_0, it is necessary to be more explicit regarding the biological interpretation of the lattice $\mathcal{L}_0$. Therefore, we now identify $\mathcal{L}_0$ with the distribution of CO blobs having a given eye preference. Such a lattice is interleaved with a second lattice of blobs having the opposite eye preference, which is given by $\mathcal{L}_0^c = \{d_0\ell_1/2 + \ell, \ell \in \mathcal{L}_0\}$. This is illustrated in Fig. 4 for a square lattice.[2] The simplest example of a periodic modulation is motivated by the experimental observation that some cells located within intermediate distances from CO blobs in primary visual cortex have very little in the way of horizontal connections [50], thus leading to an effective reduction in connectivity at the population level. The fact that CO blobs also coincide with regions in which there is a large variation in orientation preference could also lead to denser horizontal connections around blobs. This suggests introducing a spatially periodic variation in the strength of the horizontal connections of the form $J_0(\mathbf{r}|\mathbf{r}') = [1 + D(\mathbf{r})]J_0(|\mathbf{r}-\mathbf{r}'|)$ for some function D that is doubly periodic with respect to the full lattice of CO blobs $\mathcal{L} = \mathcal{L}_0 \cup \mathcal{L}_0^c$, see Fig. 4. The function $D(\mathbf{r})$ is assumed to have zero mean, that is, $\int D(\mathbf{r})\,\mathrm{d}\mathbf{r} = 0$. Combining Eqs. (2.3), (2.6) and (2.8) shows that the total weight distribution (2.3) is of the form

$$w(\mathbf{r}|\mathbf{r}') = W_0(|\mathbf{r}-\mathbf{r}'|) + \kappa[1 + D(\mathbf{r})]J(\mathbf{r}-\mathbf{r}'). \tag{2.9}$$

[2] Anatomical data indicates that the spacing between CO blobs across ocular dominance boundaries is smaller (around 350 μm) then between those in the same column (around 450 μm) [25,33,50]. This would suggest a stretching of the lattice $\mathcal{L}_0$ in the direction orthogonal to the ocular dominance columns by an approximate factor of 1.6. Interestingly, such a stretching accounts for most of the anisotropy in the distribution of patchy connections shown in Fig. 2 [6]. On the other hand, patchy feedback connections from extrastriate areas tend to be more strongly anisotropic [3]. In this paper we eliminate the stretching due to ocular dominance columns by choosing appropriately scaled planar coordinates $\mathbf{r}$. We also assume that the local connections are isotropic with respect to these scaled coordinates.

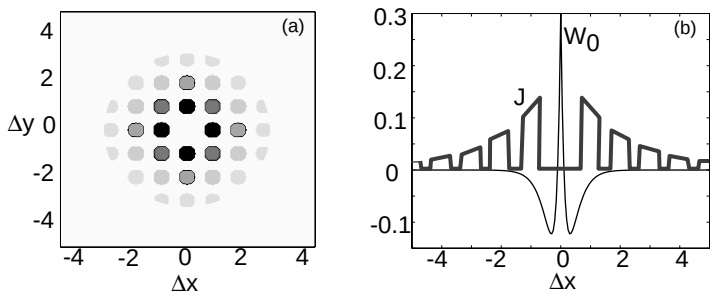

Fig. 3. (a) Contour plot of the distribution $J(\Delta\mathbf{r})$ as a function of cortical separation $\Delta\mathbf{r} = \mathbf{r} - \mathbf{r}'$ (in units of the lattice spacing d_0) showing the distribution of patchy connections on a square lattice. (b) Cross-section of J along the x-axis. An example of a local weight distribution W_0 is also shown, which is taken to be a Mexican hat function (see Eq. (3.6)).

It follows that $w(\mathbf{r}+\ell|\mathbf{r}'+\ell) = w(\mathbf{r}|\mathbf{r}')$ for all $\ell \in \mathcal{L}$ so that the weight distribution w is itself doubly periodic with respect to $\mathcal{L}$. Finally, substituting equation (2.9) into the cortical model (2.1) leads to the inhomogeneous equation

$$\frac{\partial a(\mathbf{r},t)}{\partial t} = -a(\mathbf{r},t) + \int_{\mathbf{R}^2} W_0(|\mathbf{r}-\mathbf{r}'|)\, f(a(\mathbf{r}',t))\, \mathrm{d}\mathbf{r}' + \kappa[1+D(\mathbf{r})] \int_{\mathbf{R}^2} J(\mathbf{r}-\mathbf{r}')\, f(a(\mathbf{r}',t))\, \mathrm{d}\mathbf{r}' + h_0. \tag{2.10}$$

Eq. (2.10) will be our starting point for the analysis of spontaneous cortical pattern formation in Sections 3–5. We end this section by briefly indicating how to incorporate other sources of spatially periodic variations in the pattern of horizontal connections. An alternative interpretation of the results in Ref. [50] is that there is a periodic variation in the average range of the horizontal connections. One way to implement such a scheme is to replace ξ in Eq. (2.7) by $\xi(\mathbf{r}) = \xi[1+\chi(\mathbf{r})]$ such that, for $\chi(\mathbf{r})|\mathbf{r}-\mathbf{r}'| \ll \xi$

$$J_0(\mathbf{r}|\mathbf{r}') = K\,\mathrm{e}^{-|\mathbf{r}-\mathbf{r}'|/\xi(\mathbf{r})} \approx J_0(|\mathbf{r}-\mathbf{r}'|)\left[1 + \frac{\chi(\mathbf{r})}{\xi}|\mathbf{r}-\mathbf{r}'|\right]. \tag{2.11}$$

Another source of inhomogeneity occurs when there is an anisotropy in the distribution of patchy connections that correlates with the orientation preference map [7]. This anisotropy, which is additional to any stretching associated with the ocular dominance columns, can be incorporated into our model by taking

$$J_0(\mathbf{r}|\mathbf{r}') = J_0(\chi(\mathbf{r}), T_{\theta(\mathbf{r})}[\mathbf{r}-\mathbf{r}']), \quad J_0(\chi,\mathbf{r}) = K\,\mathrm{e}^{-\sqrt{(1-\chi)^2x^2+y^2}/\xi}, \tag{2.12}$$

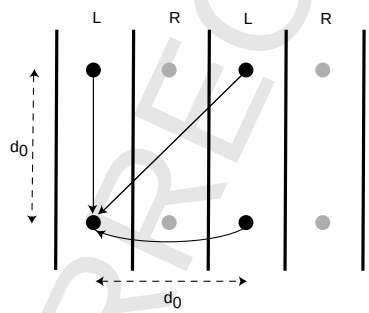

Fig. 4. Two interlocking square lattices of CO blobs (filled circles) associated respectively with left (L) and right (R) eye ocular dominance columns. Horizontal connections are assumed only to link CO blobs having the same eye preference.

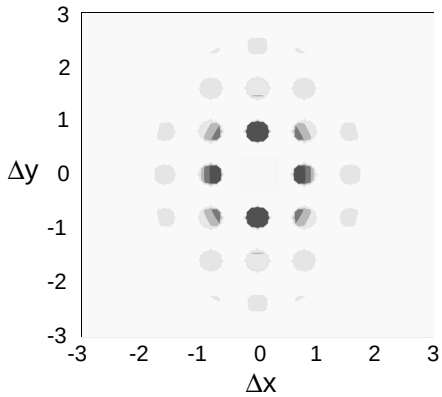

Fig. 5. Contour plot of an anisotropic distribution of patchy horizontal connections on a square lattice.

where

$$T_\theta = \begin{pmatrix} \cos\theta & -\sin\theta \\ \sin\theta & \cos\theta \end{pmatrix}. \tag{2.13}$$

Here $\chi(\mathbf{r})$ and $\theta(\mathbf{r})$ determine the eccentricity and orientation of the resulting anisotropy. They are assumed to be doubly periodic with respect to the lattice of orientation pinwheels. Assuming that $\chi|\mathbf{r}-\mathbf{r}'| \ll \xi$, we have

$$J_0(\mathbf{r}|\mathbf{r}') \approx J_0(|\mathbf{r}-\mathbf{r}'|)\left(1 + \frac{\chi(\mathbf{r})}{\xi|\mathbf{r}-\mathbf{r}'|}[\cos\theta(\mathbf{r})(x-x') - \sin\theta(\mathbf{r})(y-y')]^2\right). \tag{2.14}$$

Substituting Eq. (2.11) or (2.14) into (2.3) then leads to a generalization of Eq. (2.9) of the form

$$w(\mathbf{r}|\mathbf{r}') = W_0(|\mathbf{r}-\mathbf{r}'|) + \kappa \sum_{m=1}^{M} D_m(\mathbf{r}) J_m(\mathbf{r}-\mathbf{r}'). \tag{2.15}$$

For example, in the case of a periodically varying anisotropy, $M = 4$ with

$$D_1(\mathbf{r}) = 1, \qquad J_1(\mathbf{r}) = J(\mathbf{r}), \tag{2.16}$$

$$D_2(\mathbf{r}) = \chi(\mathbf{r})\cos^2\theta(\mathbf{r}), \qquad J_2(\mathbf{r}) = \frac{x^2}{|\mathbf{r}|\xi} J(\mathbf{r}), \tag{2.17}$$

$$D_3(\mathbf{r}) = \chi(\mathbf{r})\sin^2\theta(\mathbf{r}), \qquad J_3(\mathbf{r}) = \frac{y^2}{|\mathbf{r}|\xi} J(\mathbf{r}), \tag{2.18}$$

$$D_4(\mathbf{r}) = -2\chi(\mathbf{r})\cos\theta(\mathbf{r})\sin\theta(\mathbf{r}), \qquad J_4(\mathbf{r}) = \frac{xy}{|\mathbf{r}|\xi} J(\mathbf{r}). \tag{2.19}$$

An example of an anisotropic distribution of patchy connections is shown in Fig. 5.

3. Linear eigenvalue problem for cortical pattern formation

In this section we use perturbation methods to solve the linear eigenvalue problem for pattern forming instabilities in the presence of periodically varying inhomogeneous horizontal connections. (A preliminary version of this

analysis was briefly reported elsewhere [10].) For mathematical convenience, we impose the periodic boundary conditions $a(\mathbf{r}+L\ell_j) = a(\mathbf{r})$, $j = 1, 2$ for all $\mathbf{r} \in \mathbf{R}^2$, where L determines the effective size of cortex and ℓ_j are the generators of $\mathcal{L}_0$, see Table 1. This will not significantly affect the nature of patterns within the bulk of the medium provided that the range of cortical interactions is much smaller than L.

3.1. Homogeneous weights

Let us first consider the case of zero horizontal interactions by setting $\kappa = 0$ in Eq. (2.10) to obtain the homogeneous and isotropic network equation

$$\frac{\partial a(\mathbf{r}, t)}{\partial t} = -a(\mathbf{r}, t) + \int_{\mathbf{R}^2} W_0(|\mathbf{r} - \mathbf{r}'|)\, f(a(\mathbf{r}', t))\, \mathrm{d}\mathbf{r}' + h_0. \tag{3.1}$$

We assume that $W_0 \in L^2(\mathbf{r})$, that is, $\int_{\mathbf{R}^2} |W_0(\mathbf{r})|^2 \mathrm{d}^2\mathbf{r} < \infty$. There exists at least one fixed point solution $a(\mathbf{r}) = a_0$ of Eq. (3.1) such that

$$a_0 = \bar{W}_0 f(a_0) + h_0, \tag{3.2}$$

and $\bar{W}_0 = \int W_0(|\mathbf{r}|)\, \mathrm{d}\mathbf{r}$. If h_0 is sufficiently small relative to the threshold ζ then this fixed point is unique and stable. Under the change of coordinates $a \to a - h_0$, it can be seen that the effect of h_0 is to shift the threshold by the amount $-h_0$. Thus there are two ways to increase the excitability of the network and thus destabilize the fixed point: either by increasing the external input h_0 or reducing the threshold ζ. The latter can occur through the action of drugs on certain brain stem nuclei which provides a mechanism for generating geometric visual hallucinations [8,19]. The local stability of a_0 is found by linearization: setting $a(\mathbf{r}, t) = a_0 + \mathrm{e}^{\lambda t} a(\mathbf{r})$ and linearizing about the fixed point leads to the equation

$$\lambda a(\mathbf{r}) = -a(\mathbf{r}) + \mu \int_{\mathbf{R}^2} W_0(|\mathbf{r} - \mathbf{r}'|) a(\mathbf{r}')\, \mathrm{d}\mathbf{r}', \tag{3.3}$$

where $\mu = f'(a_0)$. Since the local weight distribution W_0 is homogeneous, it follows that the eigenmodes are in the form of plane waves $a(\mathbf{r}) = \mathrm{e}^{\mathrm{i}\mathbf{k}\cdot\mathbf{r}}$ with wavenumber $\mathbf{k}$. Substitution into Eq. (3.3) shows that the corresponding eigenvalues satisfy the dispersion relation

$$\lambda = \lambda(k) \equiv -1 + \mu \tilde{W}_0(k), \tag{3.4}$$

where $k = |\mathbf{k}|$ and $\tilde{W}_0(k)$ is the Fourier transform of $W_0(|\mathbf{r}|)$

$$\tilde{W}_0(k) = \int_{\mathbf{R}^2} W_0(|\mathbf{r}|)\, \mathrm{e}^{-\mathrm{i}\mathbf{k}\cdot\mathbf{r}}\, \mathrm{d}\mathbf{r}. \tag{3.5}$$

Given the periodic boundary conditions on a, the wavevectors $\mathbf{k}$ are constrained to lie on the lattice $\mathbf{k} = \sum_{j=1,2} (2\pi m_j/L)\hat{\ell}_j$, where $\hat{\ell}_j$, $j = 1, 2$, are the generators of the reciprocal lattice $\hat{\mathcal{L}}_0$ (see Table 1).

We can use the dispersion relation (3.4) to determine conditions under which the homogeneous state loses stability leading to the formation of spatially periodic patterns. The standard mechanism for such an instability, which is the neural analog of the Turing instability in reaction–diffusion equations, is a combination of short-range excitation and long-range inhibition [19,48]. This can be represented by the so-called "Mexican hat" function (see Fig. 6(a)):

$$W_0(r) = \frac{W_+}{2\pi\sigma_+^2}\, \mathrm{e}^{-r^2/2\sigma_+^2} - \frac{W_-}{2\pi\sigma_-^2}\, \mathrm{e}^{-r^2/2\sigma_-^2} \tag{3.6}$$

with $\sigma_+ < \sigma_- < d_0$ and $W_+\sigma_-^2 > W_-\sigma_+^2$. The corresponding Fourier transform

$$\tilde{W}_0(k) = W_+\, \mathrm{e}^{-(1/2)\sigma_+^2 k^2} - W_-\, \mathrm{e}^{-(1/2)\sigma_-^2 k^2}, \tag{3.7}$$

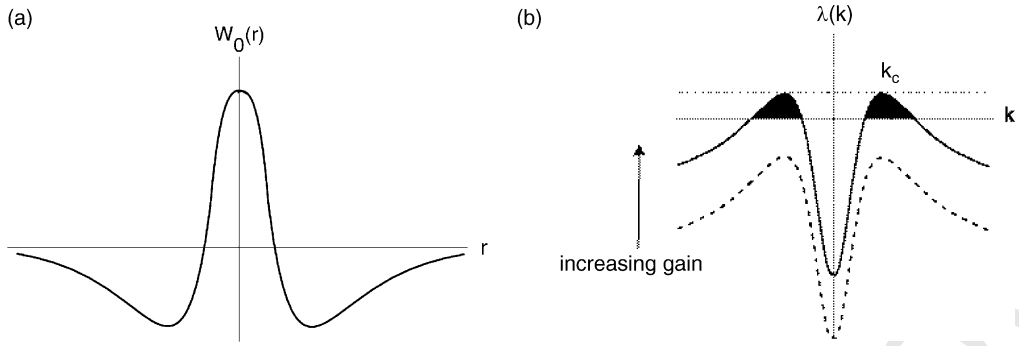

Fig. 6. Neural basis of the Turing mechanism. (a) Mexican hat interaction function showing short-range excitation and longer-range inhibition. (b) Dispersion curves $\lambda(k)$ for Mexican hat function. If the excitability μ of the cortex is increased, the dispersion curve is shifted upwards leading to a Turing instability at a critical parameter $\mu_c = \tilde{W}_0(k_c)^{-1}$, where $\tilde{W}_0(k_c) = [\max_k \tilde{W}_0(k)]$. For $\mu_c < \mu < \infty$ the homogeneous fixed point is unstable.

has a maximum at $k = k_c \neq 0$ as shown in Fig. 6(b). Since $\tilde{W}_0(k)$ is bounded, it follows that when the network is in a low activity state such that $\mu \approx 0$, any solution of Eq. (3.3) satisfies $\mathrm{Re}\,\lambda < 0$ and the fixed point is linearly stable. However, when the excitability of the network is increased, either through the action of some hallucinogen or through external stimulation, μ increases and the fixed point becomes marginally stable at the critical value μ_c, where $\mu_c^{-1} = \tilde{W}_0(k_c) \equiv \max_k\{\tilde{W}_0(k)\}$. For $\mu > \mu_c$, the fixed point is unstable and there exists a band of wavevectors $\mathbf{k}$ that have positive λ and can thus grow to form spatially varying patterns. Sufficiently close to the bifurcation point these patterns can be represented as linear combinations of plane waves

$$a(\mathbf{r}) = \sum_{n=1}^{N} (A_n\, \mathrm{e}^{\mathrm{i}\mathbf{k}_n\cdot\mathbf{r}} + A_n^*\, \mathrm{e}^{-\mathrm{i}\mathbf{k}_n\cdot\mathbf{r}}), \tag{3.8}$$

where the sum is over all wavevectors lying within some neighborhood of the critical circle $|\mathbf{k}_n| = k_c$. In the case of a large system size L, there will a large number of such excited modes. However, one usually considers regular patterns obtained by superposition of N pairs of wavevectors distributed uniformly on the critical circle, that is, $\mathbf{k}_n = \Omega_{n-1}\mathbf{k}_1$ for $n = 1, \ldots, N$ with Ω_n representing rotation through an angle π/N. The cases $N = 1, 2, 3$ correspond to roll, square and hexagonal (or triangular) patterns, respectively. Note that the solution (3.8) is defined up to a uniform translation in $\mathbf{r}$, which corresponds to phase-shifts in the complex amplitudes A_n.

The above analysis can be extended to incorporate homogeneous but nonisotropic horizontal connections by taking $\kappa > 0$ and $D(\mathbf{r}) = 0$ in Eq. (2.10). Setting

$$W(\mathbf{r}) = W_0(|\mathbf{r}|) + \kappa J(\mathbf{r}), \tag{3.9}$$

and repeating the linear stability analysis about the corresponding homogeneous fixed point, the dispersion relation (3.4) becomes

$$\lambda = \lambda(\mathbf{k}) \equiv -1 + \mu \tilde{W}(\mathbf{k}). \tag{3.10}$$

Note that $\lambda(\mathbf{k})$ now depends on the direction as well as the magnitude of $\mathbf{k}$, since it is invariant with respect to the discrete rotation symmetry group of the dual lattice $\hat{\mathcal{L}}_0$ defined in Section 2 (see Table 1), rather than the continuous rotation group. It follows that a particular wavevector $\mathbf{k}^*$ will be selected by the Turing mechanism, together with all modes generated by discrete rotations of the dual lattice (ignoring accidental degeneracies). The eigenmodes will naturally tend to be low-dimensional patterns such as rolls and hexagons, that is, they will satisfy

Eq. (3.8) with $\mathbf{k}_n = \Omega_{n-1}\mathbf{k}^*$ for $n = 2, \ldots, N$ and $N = 2$ if $\mathcal{L}_0$ is a square lattice or $N = 3$ if $\mathcal{L}_0$ is a hexagonal lattice. Thus the existence of a lattice $\mathcal{L}_0$ underlying the distribution of patchy horizontal connections provides a physical mechanism for generating low-dimensional, doubly periodic patterns. Such cortical activity patterns are of particular interest, since they provide a possible explanation for the occurrence of certain basic types of geometric visual hallucinations [8,19]. (In Euclidean symmetric models of cortical pattern formation, the double-periodicity of the solutions is imposed by hand as a mathematical simplification rather than reflecting the existence of a real lattice [8,19,21].)

3.2. Inhomogeneous weights

Now suppose that there exists a spatially periodic variation in the strength of horizontal connections as specified by the function $D(\mathbf{r})$ in Eq. (2.10). For the sake of simplicity, we will assume here that D is doubly periodic with respect to the lattice $\mathcal{L} = \{(m_1\ell_1 + m_2\ell_2)d : m_1, m_2 \in \mathbf{Z}\}$ with the same lattice spacing $d = d_0/2$ in both directions ℓ_1, ℓ_2; the analysis is easily extended to the more general case illustrated in Fig. 4. Under this simplification the lattices $\mathcal{L}$ and $\mathcal{L}_0$ have the same discrete rotation symmetry group. The first point to note is that Eq. (2.10) no longer has a homogeneous fixed point solution. However, by introducing an appropriate inhomogeneity in the external input, $h_0 \to h(\mathbf{r})$, it is possible to recover such a solution. Linearization then leads to the eigenvalue equation

$$\lambda a(\mathbf{r}) = -a(\mathbf{r}) + \mu \int_{\mathbf{R}^2} w(\mathbf{r}|\mathbf{r}')a(\mathbf{r}')\,\mathrm{d}\mathbf{r}' \tag{3.11}$$

with w given by Eq. (2.9). [Note that we could also linearize about the inhomogeneous fixed point associated with a constant input h_0: this would simply introduce additional doubly periodic contributions to the eigenvalue equation.] The double-periodicity of $\mathcal{D}$ implies that

$$w(\mathbf{r} + \ell|\mathbf{r}') = w(\mathbf{r}|\mathbf{r}' - \ell) \quad \text{for all } \ell \in \mathcal{L}. \tag{3.12}$$

From this relation it follows that the solutions of Eq. (3.11) are of the form[3]

$$a_{\mathbf{k}}(\mathbf{r}) = \mathrm{e}^{\mathrm{i}\mathbf{k}\cdot\mathbf{r}} u_{\mathbf{k}}(\mathbf{r}) \tag{3.13}$$

with $u_{\mathbf{k}}(\mathbf{r} + \ell) = u_{\mathbf{k}}(\mathbf{r})$ for all $\ell \in \mathcal{L}$. In order to prove this, let us introduce the translation operator T_ℓ such that $T_\ell f(\mathbf{r}) = f(\mathbf{r} + \ell)$ for any function f. Then

$$\begin{aligned} T_\ell \int_{\mathbf{R}^2} w(\mathbf{r}|\mathbf{r}')a(\mathbf{r}')\,\mathrm{d}\mathbf{r}' &= \int_{\mathbf{R}^2} w(\mathbf{r} + \ell|\mathbf{r}')a(\mathbf{r}')\,\mathrm{d}\mathbf{r}' = \int_{\mathbf{R}^2} w(\mathbf{r}|\mathbf{r}' - \ell)a(\mathbf{r}')\,\mathrm{d}\mathbf{r}' \\ &= \int_{\mathbf{R}^2} w(\mathbf{r}|\mathbf{r}')a(\mathbf{r}' + \ell)\,\mathrm{d}\mathbf{r}' = \int_{\mathbf{R}^2} w(\mathbf{r}|\mathbf{r}')T_\ell a(\mathbf{r}')\,\mathrm{d}\mathbf{r}'. \end{aligned} \tag{3.14}$$

Defining the linear operator $\hat{\mathcal{H}}$ according to

$$\hat{\mathcal{H}}a(\mathbf{r}) = -a(\mathbf{r}) + \mu \int_{\mathbf{R}^2} w(\mathbf{r}|\mathbf{r}')a(\mathbf{r}')\,\mathrm{d}\mathbf{r}', \tag{3.15}$$

we have $T_\ell\hat{\mathcal{H}} = \hat{\mathcal{H}}T_\ell$. Shur's lemma then implies that $\hat{\mathcal{H}}$ and T_ℓ have simultaneous eigensolutions:

$$\hat{\mathcal{H}}a = \lambda a, \qquad T_\ell a = C(\ell)a. \tag{3.16}$$

[3] In condensed matter physics solutions of Schrodinger's equation for an electron in a periodic potential take this form and are called Bloch waves [1]. Bloch waves are spatial analogs of the eigenfunctions arising in Floquet theory.

Since $T_\ell T_{\ell'} = T_{\ell+\ell'}$, we have

$$C(\ell)C(\ell') = C(\ell+\ell'), \tag{3.17}$$

which implies that $C(\ell) = \mathrm{e}^{\mathrm{i}\mathbf{k}\cdot\ell}$ and the result follows.

Another way to establish the general form of the eigensolutions (3.13) is to introduce the Fourier series expansions

$$D(\mathbf{r}) = \sum_{\mathbf{q}} \mathcal{D}_{\mathbf{q}}\, \mathrm{e}^{\mathrm{i}\mathbf{q}\cdot\mathbf{r}}, \qquad \mathbf{q} = \sum_{j=1,2} \frac{2\pi n_j}{d}\hat{\ell}_j, \tag{3.18}$$

and

$$a(\mathbf{r}) = \frac{1}{L^2}\sum_{\mathbf{k}} a_{\mathbf{k}}\, \mathrm{e}^{\mathrm{i}\mathbf{k}\cdot\mathbf{r}}, \qquad \mathbf{k} = \sum_{j=1,2} \frac{2\pi m_j}{L}\hat{\ell}_j, \tag{3.19}$$

where $\hat{\ell}_j$, $j = 1, 2$, are the generators of the reciprocal lattice $\hat{\mathcal{L}}$ (see Table 1). Eq. (3.11) then reduces to

$$[\lambda + 1 - \mu\tilde{W}_0(k)]a_{\mathbf{k}} = \kappa \sum_{\mathbf{q}} \mathcal{V}_{\mathbf{q}}(\mathbf{k})a_{\mathbf{k}-\mathbf{q}}, \tag{3.20}$$

where

$$\mathcal{V}_{\mathbf{q}}(\mathbf{k}) = \tilde{J}(\mathbf{k}-\mathbf{q})[\delta_{\mathbf{q},0} + \mathcal{D}_{\mathbf{q}}], \tag{3.21}$$

and $\tilde{J}(\mathbf{k})$ is the Fourier transform of $J(\mathbf{r})$. Eq. (3.20) implies that the lateral interactions only couple together those coefficients $a_{\mathbf{k}}, a_{\mathbf{k}-\mathbf{q}}, a_{\mathbf{k}-\mathbf{q}'}, \ldots$ whose wavevectors differ by a reciprocal lattice vector. In other words, if we fix $\mathbf{k}$ then

$$a(\mathbf{r}) = \sum_{\mathbf{q}} a_{\mathbf{k}-\mathbf{q}}\, \mathrm{e}^{\mathrm{i}(\mathbf{k}-\mathbf{q})\cdot\mathbf{r}} = \mathrm{e}^{\mathrm{i}\mathbf{k}\cdot\mathbf{r}} u(\mathbf{r}), \tag{3.22}$$

which is of the form (3.13) with $u(\mathbf{r})$ given by the periodic function

$$u(\mathbf{r}) = \sum_{\mathbf{q}} a_{\mathbf{k}-\mathbf{q}}\, \mathrm{e}^{-\mathrm{i}\mathbf{q}\cdot\mathbf{r}}. \tag{3.23}$$

3.3. Perturbation theory

It is generally not possible to find exact solutions of the eigenvalue equation (3.20). Therefore, we proceed by carrying out a perturbation expansion with respect to the small parameter κ that characterizes the relative weakness of the horizontal connections.[4] Let k_{c} be the critical wavenumber for a pattern forming instability when $\kappa = 0$. We also define $\mathcal{N}_\kappa(k_{\mathrm{c}})$ to be a small neighborhood of the critical circle $|\mathbf{k}| = k_{\mathrm{c}}$. We then have to distinguish between two cases, based on whether or not the following degeneracy condition holds: there exists a reciprocal lattice vector $\mathbf{Q}$ such that

$$|\tilde{W}_0(k) - \tilde{W}_0(|\mathbf{k}-\mathbf{Q}|)| = \mathcal{O}(\kappa), \quad \mathbf{k} \in \mathcal{N}_\kappa(k_{\mathrm{c}}), \tag{3.24}$$

and $\tilde{W}_0(k) - \tilde{W}_0(|\mathbf{k}-\mathbf{q}|)| \gg \kappa$ for all $\mathbf{q} \in \hat{\mathcal{L}}$ such that $\mathbf{q} \neq \mathbf{Q}$. Note that the exact degeneracy condition $\tilde{W}_0(k) = \tilde{W}_0(|\mathbf{k}-\mathbf{Q}|)$ is only satisfied if $|\mathbf{k}| = |\mathbf{k}-\mathbf{Q}|$. This means that $\mathbf{k}$ must lie on the perpendicular bisector of the line joining the origin of the reciprocal lattice $\hat{\mathcal{L}}$ to the lattice point $\mathbf{Q}$, as illustrated in Fig. 7(a). Another

[4] The perturbation analysis is similar in structure to that used to solve the Schrodinger equation in a *weak* periodic potential [1].

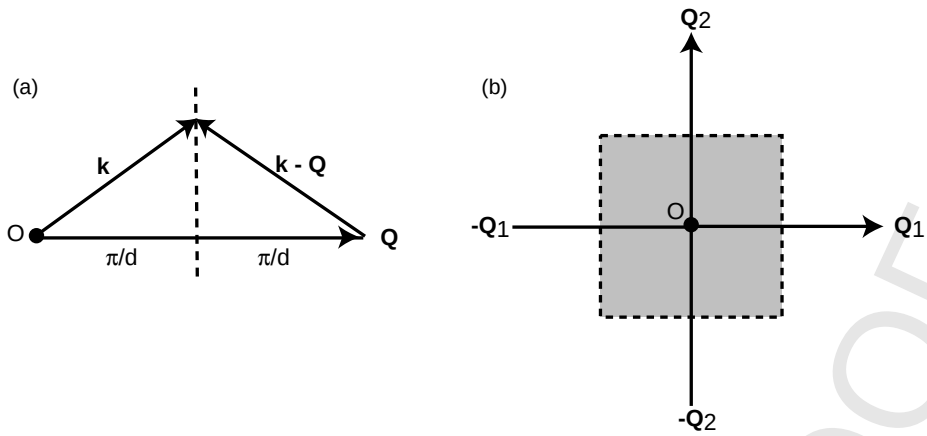

Fig. 7. (a) If $k = |\mathbf{k} - \mathbf{Q}|$ then $\mathbf{k}$ must lie on the bisector of the reciprocal lattice vector $\mathbf{Q}$. (b) Construction of the first Brillouin zone (shaded region) in the reciprocal square lattice with $\mathbf{Q}_j = 2\pi\hat{\ell}_j/d$.

useful concept is that of a Brillouin zone [1]. The first Brillouin zone is the fundamental domain around the origin of the reciprocal lattice formed by the perpendicular bisectors of the shortest lattice vectors (of length $2\pi/d$). The example of a square lattice is shown in Fig. 7(b). The higher-order Brillouin zones are similarly constructed using the perpendicular bisectors of larger lattice vectors. It follows that any point on the boundary of a Brillouin zone will satisfy the exact degeneracy condition.

Nondegenerate case. First, suppose that Eq. (3.24) does not hold, that is, if $\mathbf{k} \in \mathcal{N}_\kappa(k_c)$ then $|\tilde{W}_0(k) - \tilde{W}_0(\mathbf{k}-\mathbf{q})| \gg \kappa$ for all $\mathbf{q} \in \hat{\mathcal{L}}$, $\mathbf{q} \neq 0$. This occurs, for example, if the critical circle lies well within the first Brillouin zone, see Fig. 8(a). We then fix $\mathbf{k}$ and look for solutions satisfying $a_{\mathbf{k}} \to 1$ and $a_{\mathbf{k}-\mathbf{q}} \to 0$, $\mathbf{q} \neq 0$, in the limit $\kappa \to 0$. This corresponds to a small perturbation of the plane wave state $e^{i\mathbf{k}\cdot\mathbf{r}}$. Eq. (3.20) implies that (for $\mathbf{q} \neq 0$)

$$[\lambda + 1 - \mu\tilde{W}_0(|\mathbf{k} - \mathbf{q}|)]a_{\mathbf{k}-\mathbf{q}} = \kappa \sum_{\mathbf{q}'} \mathcal{V}_{\mathbf{q}'}(\mathbf{k} - \mathbf{q})a_{\mathbf{k}-\mathbf{q}-\mathbf{q}'}, \tag{3.25}$$

which can be rewritten in the form

$$a_{\mathbf{k}-\mathbf{q}} = \kappa \frac{\mathcal{V}_{-\mathbf{q}}(\mathbf{k} - \mathbf{q})a_{\mathbf{k}}}{\lambda + 1 - \mu\tilde{W}_0(|\mathbf{k} - \mathbf{q}|)} + \kappa \sum_{\mathbf{q}'\neq 0} \frac{\mathcal{V}_{\mathbf{q}'-\mathbf{q}}(\mathbf{k} - \mathbf{q})a_{\mathbf{k}-\mathbf{q}'}}{\lambda + 1 - \mu\tilde{W}_0(|\mathbf{k} - \mathbf{q}|)}. \tag{3.26}$$

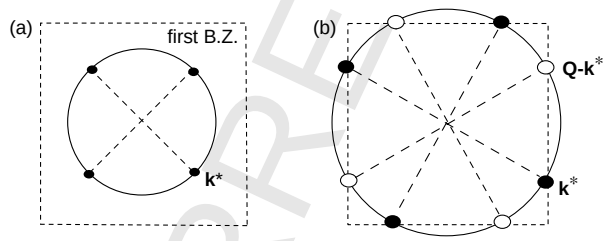

Fig. 8. Selected wavevectors on the critical circle for a square lattice. (a) Nondegenerate case: the critical circle lies well within the first Brillouin zone. (b) Degenerate case: the critical circle intersects the border of the first Brillouin zone and there is a doubling up of the marginally stable modes.

The first term on the right-hand side will be an order of magnitude larger than the remaining terms provided that the degeneracy condition (3.24) does not hold. Therefore

$$a_{\mathbf{k}-\mathbf{q}} = \kappa \frac{\mathcal{V}_{-\mathbf{q}}(\mathbf{k}-\mathbf{q})a_{\mathbf{k}}}{\lambda + 1 - \mu \tilde{W}_0(|\mathbf{k}-\mathbf{q}|)} + \mathcal{O}(\kappa^2). \tag{3.27}$$

Substituting this back into Eq. (3.20) gives

$$[\lambda + 1 - \mu \tilde{W}_0(k)]a_{\mathbf{k}} = \kappa \mathcal{V}_0(\mathbf{k})a_{\mathbf{k}} + \kappa^2 \sum_{\mathbf{q}\neq 0} \frac{\mathcal{V}_{\mathbf{q}}(\mathbf{k})\mathcal{V}_{-\mathbf{q}}(\mathbf{k}-\mathbf{q})a_{\mathbf{k}}}{\lambda + 1 - \mu \tilde{W}_0(|\mathbf{k}-\mathbf{q}|)} + \mathcal{O}(\kappa^3). \tag{3.28}$$

Hence, replacing the denominator by the lowest-order contribution yields

$$\lambda(\mathbf{k}) = -1 + \mu \tilde{W}_0(k) + \kappa \mathcal{V}_0(\mathbf{k}) + \kappa^2 \sum_{\mathbf{q}\neq 0} \frac{\mathcal{V}_{\mathbf{q}}(\mathbf{k})\mathcal{V}_{-\mathbf{q}}(\mathbf{k}-\mathbf{q})}{\mu[\tilde{W}_0(k) - \tilde{W}_0(|\mathbf{k}-\mathbf{q}|)]} + \mathcal{O}(\kappa^3). \tag{3.29}$$

To leading order in κ, the marginally stable modes will be those modes on the critical circle that maximize the term $\mathcal{V}_0(\mathbf{k})$. Since $\mathcal{V}_0(\mathbf{k})$ is invariant with respect to discrete rotations of the dual lattice $\hat{\mathcal{L}}$, a particular wavevector $\mathbf{k}^*$ on the critical circle will be selected together with all modes generated by discrete rotations of the lattice. This is illustrated in Fig. 8(a) for the square lattice. The eigenmodes will thus be of the form

$$a(\mathbf{r}) = \sum_{i=1,\dots,N} u_i(\mathbf{r})\, \mathrm{e}^{\mathrm{i}\mathbf{k}_i\cdot\mathbf{r}} + \text{c.c.} \tag{3.30}$$

with

$$u_i(\mathbf{r}) = c_i \left[1 + \kappa \sum_{\mathbf{q}\neq 0} \mathrm{e}^{-\mathrm{i}\mathbf{q}\cdot\mathbf{r}} \frac{\mathcal{V}_{-\mathbf{q}}(\mathbf{k}-\mathbf{q})}{\mu(\tilde{W}_0(k) - \tilde{W}_0(|\mathbf{k}-\mathbf{q}|))} + \mathcal{O}(\kappa^2) \right]. \tag{3.31}$$

Here $N = 2$ for the square lattice with $\mathbf{k}_1 = \mathbf{k}^*$ and $\mathbf{k}_2 = R_{\pi/2}\mathbf{k}^*$, where R_θ denotes rotation through an angle θ. Similarly, $N = 3$ for the hexagonal lattice with $\mathbf{k}_1 = \mathbf{k}^*$, $\mathbf{k}_2 = R_{2\pi/3}\mathbf{k}^*$ and $\mathbf{k}_3 = R_{4\pi/3}\mathbf{k}^*$.

Degenerate case. Now suppose that the degeneracy condition (3.24) is satisfied for some $\mathbf{Q} \in \hat{\mathcal{L}}$, which implies that the critical circle is close to a Brillouin zone boundary, see Fig. 8(b). This implies that there is an approximate twofold degeneracy,[5] and we must treat Eq. (3.20) separately for the two cases $\mathbf{k}$ and $\mathbf{k}-\mathbf{Q}$. Thus, to first-order in κ, Eq. (3.20) reduces to a pair of equations for the coefficients $a_{\mathbf{k}}$ and $a_{\mathbf{k}-\mathbf{Q}}$:

$$\begin{pmatrix} \lambda - E(\mathbf{k}) & \kappa\mathcal{V}_{\mathbf{Q}}(\mathbf{k}) \\ \kappa\mathcal{V}_{-\mathbf{Q}}(\mathbf{k}-\mathbf{Q}) & \lambda - E(\mathbf{k}-\mathbf{Q}) \end{pmatrix} \begin{pmatrix} a_{\mathbf{k}} \\ a_{\mathbf{k}-\mathbf{Q}} \end{pmatrix} = 0, \tag{3.32}$$

where $E(\mathbf{k}) = -1 + \mu[\tilde{W}_0(k) + \kappa\mathcal{V}_0(\mathbf{k})]$. Assume for the moment that the exact degeneracy condition $\tilde{W}_0(k) = \tilde{W}_0(|\mathbf{k}-\mathbf{Q}|)$ holds so that $\mathbf{k}$ is on a Brillouin zone boundary. As a further simplification, let $\tilde{J}(\mathbf{k}-\mathbf{q}) = \tilde{J}(\mathbf{k})$ for all $\mathbf{q} \in \hat{\mathcal{L}}$ so that $E(\mathbf{k}-\mathbf{Q}) = E(\mathbf{k})$. This is a good approximation when the patch size $\mathcal{P}_0$ is small. Taking $D(\mathbf{r})$ to be a real, even function of $\mathbf{r}$ so that $\mathcal{D}_{\mathbf{Q}} = \mathcal{D}_{-\mathbf{Q}}$, it also follows that $\mathcal{V}_{-\mathbf{Q}}(\mathbf{k}-\mathbf{Q}) = \mathcal{V}_{\mathbf{Q}}(\mathbf{k})$. The above matrix equation then has solutions of the form

$$\lambda_{\pm}(\mathbf{k}) = -1 + \mu(\tilde{W}_0(k) + \kappa[\mathcal{V}_0(\mathbf{k}) \pm \mathcal{V}_{\mathbf{Q}}(\mathbf{k})]) \tag{3.33}$$

[5] It is also possible to have a higher-fold degeneracy with $|\tilde{W}_0(k) - \tilde{W}_0(|\mathbf{k}-\mathbf{Q}_m|)| = \mathcal{O}(\kappa)$ for a set of reciprocal lattice vectors $\mathcal{Q}_m$, $m = 1, \dots, M$. The analysis is easily generalized to this case.

with $a_{\mathbf{k}-\mathbf{Q}} = \pm a_{\mathbf{k}}$. Thus there is a splitting into even and odd eigenmodes

$$a^{\pm}_{\mathbf{k}}(\mathbf{r}) = \mathrm{e}^{\mathrm{i}\mathbf{k}\cdot\mathbf{r}} \pm \mathrm{e}^{\mathrm{i}(\mathbf{k}-\mathbf{Q})\cdot\mathbf{r}}. \tag{3.34}$$

(If $\mathbf{k}$ is close to, but not on, the Brillouin zone boundary, there will be a slight mixing between the even and odd eigenmodes—this will not modify our conclusions significantly.) Let $\mathbf{k}_{\pm}$ denote global maxima of the functions $\lambda_{\pm}(\mathbf{k})$ and set $\mathbf{k}^* = \mathbf{k}_+$ if $\lambda_+(\mathbf{k}_+) > \lambda_-(\mathbf{k}_-)$ and $\mathbf{k}^* = \mathbf{k}_-$ otherwise. It follows that the marginally stable eigenmodes will be of the approximate form $a(\mathbf{r}) = \sum_{j=1,\dots,N} A_j a^{\pm}_{\mathbf{k}_j}(\mathbf{r}) + \text{c.c.}$ with $\mathbf{k}_1 = \mathbf{k}^*$ and $\mathbf{k}_j$, $j = 2, \dots, N$, related to $\mathbf{k}^*$ by discrete rotations of the lattice. Even $(+)$ modes will be selected when $\mathbf{k}^* = \mathbf{k}_+$ and odd $(-)$ modes when $\mathbf{k}^* = \mathbf{k}_-$.

3.4. Pinning of cortical patterns

We conclude from the above perturbation analysis that for certain critical wavenumbers k_{c} the resulting cortical activity patterns are pinned to the underlying lattice $\mathcal{L}$. This follows from the structure of the even and odd solutions (3.34), which are in the form of standing waves whose amplitudes vary as $\cos(\mathbf{Q}\cdot\mathbf{r}/2)$ and $\sin(\mathbf{Q}\cdot\mathbf{r}/2)$, respectively. Consider, for example, the simple case of a roll pattern along the x-axis with $\mathbf{k}^* = (k_{\mathrm{c}}, 0)$ and a square reciprocal lattice $\hat{\mathcal{L}}$ with generators $\hat{\ell}_1 = (d^{-1}, 0)$ and $\hat{\ell}_2 = (0, d^{-1})$, where d is the lattice spacing. If $k_{\mathrm{c}} = \pi/d$ then $\mathbf{Q} = (2\pi/d, 0)$ and the even/odd modes are of the form

$$a^{+}(x) = \cos\left(\tfrac{1}{2}k_{\mathrm{c}}x\right), \quad a^{-}(x) = \sin\left(\tfrac{1}{2}k_{\mathrm{c}}x\right). \tag{3.35}$$

Thus the even mode has extrema at sites on the lattice $\mathcal{L}$ (corresponding to CO blobs, say) whereas the odd mode has extrema between lattice sites (corresponding to inter-blobs, say). This is illustrated in Fig. 9 for a one-dimensional lattice. One might have expected the activity patterns in Fig. 9 to have their *maxima* at the CO blobs, since the latter are supposed to be sites of higher metabolic activity. However, it should be remembered that the staining of the blobs to CO occurs under conditions of normal vision. Thus the primary source of higher activity in this case is due to the external drive from the lateral geniculate nucleus (LGN) induced by visual stimuli. In this paper, on the other hand, we are considering spontaneous cortical activity in the absence of any visual stimuli. Thus, in the case of homogeneous cortical interactions, there is no intrinsic mechanism for ensuring that the peaks of spontaneous activity coincide with the CO blobs. We have shown that inhomogeneities in the horizontal connections that correlate with the distribution of CO blobs can break translation symmetry in such a way as to pin the activity pattern to the blobs along the lines of Fig. 9.

The above result raises two important issues. First, under what circumstances will the wavenumber of the primary pattern lie close to a Brillouin zone boundary so that pinning occurs? Second, to what extent does the pinning of the pattern to the lattice $\mathcal{L}$ persist when nonlinearities are included? We will investigate the first issue in the remainder of this section and address the second issue in Sections 4 and 5. In order to proceed, it is useful to consider a slightly

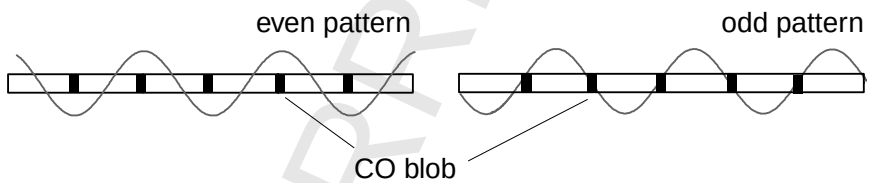

Fig. 9. Even and odd eigenmodes localized around blob and inter-blob regions.

different form of the homogeneous patchy weight distribution $J(\mathbf{r})$ given by Eq. (2.6):

$$J(\mathbf{r}) = \sum_{\ell \in \mathcal{L}_0, \ell \neq 0} J_0(|\mathbf{r}|) G(\mathbf{r} - \ell), \tag{3.36}$$

where G is a localized function that determines the size and shape of an individual horizontal patch. For simplicity, consider the limiting case in which the patch size is infinitesimal such that $G(\mathbf{r}) \to \delta(\mathbf{r})$. The basic idea can now be illustrated by considering a one-dimensional version with

$$J(x) = \sum_{n \neq 0} J_0(nd_0) \delta(x - nd_0), \tag{3.37}$$

where d_0 is the patch spacing (see Section 2). Taking the one-dimensional Fourier transform of J gives

$$\tilde{J}(k) = \sum_{n \neq 0} J_0(nd_0)\, \mathrm{e}^{-\mathrm{i}knd_0}. \tag{3.38}$$

In the case of the exponential function (2.7) with $K = 1$, the sum over lattice sites may be performed explicitly to yield

$$\tilde{J}(k) = \frac{\mathrm{e}^{d_0/\xi} \cos(kd_0) - 1}{[\mathrm{e}^{d_0/\xi} \cos(kd_0) - 1]^2 + [\mathrm{e}^{d_0/\xi} \sin(kd_0)]^2}. \tag{3.39}$$

It follows that for infinitesimal patch size, the Fourier transform of the homogeneous part of the horizontal weight distribution is a $(2\pi/d_0)$-periodic function of k and thus has an infinite set of global maxima and global minima. This infinite degeneracy is then broken by the local connections resulting in dispersion curves such as shown in Fig. 10. Given the range of the local connections W_0, the maximum of $\tilde{W}(k)$ is likely to occur close to the peak $k_c \approx 2\pi/d_0$. Finally, recall from Section 2 that the lattice spacing d_0 of the patchy horizontal connections may differ from the periodicity d of the inhomogeneity $D(\mathbf{r})$. This is illustrated in Fig. 4 for the case of CO blobs. Thus, in our one-dimensional example it is possible that $d_0 = 2d$ and hence $k_c \approx \pi/d$. Note that the above argument is easily extended to the case of finite patch size: there is simply an additional factor $\tilde{G}(k)$ multiplying the second term on the right-hand side of Eq. (3.39).

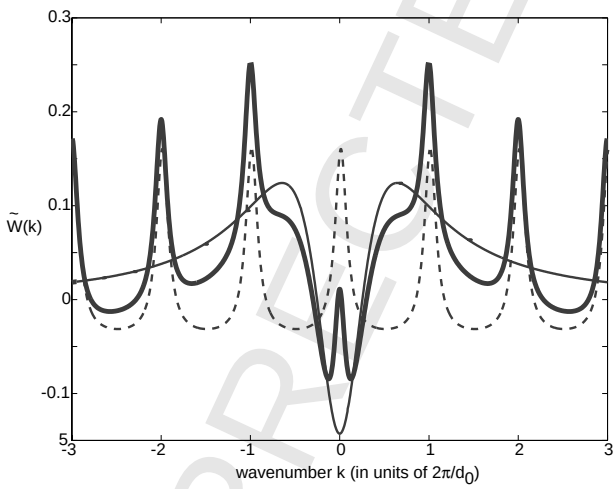

Fig. 10. Thin solid curve: Fourier transform $\tilde{W}_0(k)$ of a local Mexican hat weight distribution. Dashed curve: Fourier transform $\tilde{J}(k)$ of long-range weight distribution satisfying Eq. (3.39) with $\xi = 2d_0$. Thick solid curve: Fourier transform of the total weight distribution $\tilde{W}(k) = \tilde{W}_0(k) + \kappa \tilde{J}(k)$ for $\kappa = 0.25$.

4. Multiple scale analysis of nonlocal cortical model

In order to investigate the saturation, stabilization and selection of cortical patterns beyond the primary bifurcation point, it is necessary to carry out a nonlinear analysis of Eq. (2.10). In the vicinity of the bifurcation point, one can exploit a separation of time and space scales to derive a Ginzburg amplitude equation for the primary pattern along analogous lines to the analysis of fluid convection patterns [17,18,35,40,46]. However, the analysis of cortical patterns is complicated by the fact that the underlying integro-differential equation (2.10) is nonlocal in space. In this section we develop a multiple scale perturbation expansion of this equation that takes into account the nonlocal nature of the neuronal interactions. Note that previous studies of cortical pattern formation have focused on the selection and stability of *uniform* amplitude roll, square and hexagonal patterns [12,19,21]. The analysis presented here extends this work by taking into account slow spatial phase modulations of the amplitude. It is well known from fluid convection that diffusion-induced long-wavelength phase modulations of primary patterns can induce secondary instabilities away from the bifurcation point [17,18,46]. A major reason for being interested in these phase instabilities in the case of the cortical model (2.10) is that they can couple to weak, spatially periodic variations in the strength of the horizontal connections as specified by the function $D(\mathbf{r})$. Such a coupling provides a nonlinear mechanism for pinning the pattern to the underlying cortical lattice, as explained in Section 5.

4.1. Method of multiple scales

For simplicity, we will restrict our analysis to spatial modulations of a roll pattern that are parallel to the critical wavevector, which is chosen to be in the x-direction. Since the amplitude of the pattern is then y-independent, Eq. (2.10) can effectively be reduced to the one-dimensional system

$$\frac{\partial a(x,t)}{\partial t} = -a(x,t) + \int W(x-x')\, f(a(x',t))\, \mathrm{d}x' + \kappa D(x) \int J(x-x')\, f(a(x',t))\, \mathrm{d}x' + h_0. \tag{4.1}$$

Here $W(x) = \int_{\mathbf{R}} W(\mathbf{r})\, \mathrm{d}y$, $J(x) = \int_{\mathbf{R}} J(\mathbf{r})\, \mathrm{d}y$ and $D(x) = L^{-1} \int_0^L D(\mathbf{r})\, \mathrm{d}y$. Let $a(x,t) = a_0$ be a homogeneous fixed point solution of Eq. (4.1) when $\kappa = 0$ (homogeneous horizontal connections). Linearizing about the fixed point leads to the dispersion relation

$$\lambda(k) = -1 + \mu \tilde{W}(k), \tag{4.2}$$

where $\tilde{W}(k)$ is the Fourier transform of the weight distribution $W(x)$. Suppose that the fixed point undergoes a primary pattern forming instability at the critical parameter value $\mu = \mu_c$, where $\mu_c^{-1} = \tilde{W}(k_c)$. Expanding the dispersion equation about the critical wavenumber k_c and using the fact that $\tilde{W}(k_c)$ is a maximum gives

$$\lambda(k) = -1 + (\mu_c + \Delta\mu)\left(\tilde{W}(k_c) + \frac{1}{2}(k-k_c)^2 \frac{\mathrm{d}^2 \tilde{W}}{\mathrm{d}k^2}(k_c) + \cdots\right) = \Delta\mu \tilde{W}(k_c) - \alpha(k-k_c)^2 + \cdots, \tag{4.3}$$

where $\Delta\mu = \mu - \mu_c$ and $\alpha = -\mu_c \tilde{W}_0''(k_c)/2 > 0$. Introducing the small parameter ε and setting $\Delta\mu = \varepsilon^2$ we see that the unstable modes occupy a band of width $\mathcal{O}(\varepsilon)$ and the rate of growth of the patterns is $\mathcal{O}(\varepsilon^2)$. The interaction of two or more modes within the unstable band gives rise to a spatial modulation of the periodic pattern on a length-scale that is $\mathcal{O}(1/\varepsilon)$ compared to the pattern wavelength $2\pi/k_c$. Within a multiple scale perturbation expansion this suggests introducing a slow spatial scale $X = \varepsilon x$. Similarly, the slow growth rate of the patterns implies that there is a slow time scale $T = \varepsilon^2 t$. Given these slow spatial and temporal scales, we define the following

multiple scale version of the integro-differential evolution Eq. (4.1):

$$\varepsilon^2 \frac{\partial a(x, X, T)}{\partial T} = -a(x, X, T) + \int W(x - x') f(a(x', X + \varepsilon(x' - x), T))\, \mathrm{d}x' + \kappa D(x) \int J(x - x') f(a(x', X + \varepsilon(x' - x), T))\, \mathrm{d}x' + h_0. \tag{4.4}$$

Note that we have explicitly taken into account the nonlocal shift in the slow spatial coordinate X by an amount $\varepsilon(x' - x)$. The particular form of Eq. (4.4) is motivated by the observation that it satisfies the following two properties: (i) a perturbation expansion in ε reproduces the dispersion relation (4.3); (ii) in the case of exponential weights it reduces to an equivalent multiple scale differential equation (see Appendix A).

In order to carry out a perturbation expansion of Eq. (4.4), we have to specify the ε-dependence of the inhomogeneity D and the coupling κ. For concreteness, we consider the periodic function $D(x) = D_0[\mathrm{e}^{2\pi \mathrm{i} x/d} + \mathrm{e}^{-2\pi \mathrm{i} x/d}]$ with the lattice spacing d satisfying the *near-resonance* condition

$$\frac{2\pi}{d} = \frac{n}{m}(k_\mathrm{c} + \varepsilon q), \quad n \neq m \tag{4.5}$$

for integers n, m. If $q \equiv 0$ then the lattice spacing d is rationally related to the critical wavelength of the roll pattern. The amplitude D_0 of the spatial inhomogeneity can be absorbed into κ so that, in terms of fast and slow variables

$$D(x, X) = \mathrm{e}^{\mathrm{i} n k_\mathrm{c} x/m}\, \mathrm{e}^{\mathrm{i} n q X/m} + \text{c.c.} \tag{4.6}$$

Given this form for D, we carry out a perturbation expansion of Eq. (4.4) in three distinct coupling regimes: (i) $\kappa = 0$; (ii) $\kappa = \mathcal{O}(\varepsilon^2)$; (iii) $\kappa = \mathcal{O}(\varepsilon)$. The smallness of κ reflects both the relative strength of the horizontal connections and the amplitude of the inhomogeneity. In each case we substitute the series expansion

$$a = a_0 + \varepsilon a_1 + \varepsilon^2 a_2 + \varepsilon^3 a_3 + \cdots \tag{4.7}$$

into Eq. (4.4) and expand the firing-rate function $f(a)$ as a Taylor series about a_0

$$f(a) = f(a_0) + \mu(a - a_0) + g_2(a - a_0)^2 + g_3(a - a_0)^3 + \cdots, \tag{4.8}$$

where $g_2 = f''(a_0)/2$, $g_3 = f'''(a_0)/6$. We also expand $a_n(x', X + \varepsilon(x' - x), T)$ as a Taylor series in powers of $\varepsilon(x' - x)$. Finally, we collect terms at successive orders of ε to obtain a hierarchy of equations for the components $a_n(x, X, T)$; solvability conditions arising from the higher-order equations then determine the amplitude equation for the slow behavior of the critical mode a_1:

$$a_1(x, X, T) = A(X, T)\, \mathrm{e}^{\mathrm{i} k_\mathrm{c} x} + A^*(X, T)\, \mathrm{e}^{-\mathrm{i} k_\mathrm{c} x}, \tag{4.9}$$

where $A(X, T)$ represents a slowly varying envelope of the roll pattern. Assuming the near-resonance condition (4.5), we show that the amplitude equation in the presence of weak spatially periodic modulated horizontal connections takes the general form

$$\frac{\partial A}{\partial T} = \omega A + \alpha \frac{\partial^2 A}{\partial X^2} - \beta |A|^2 A + \gamma A^{*n-1}\, \mathrm{e}^{\mathrm{i} n q X}, \tag{4.10}$$

where $\gamma \sim \kappa^m$.

An amplitude equation of the form (4.10) was previously derived within the context of fluid convection under external periodic forcing [15], where it was used to investigate commensurate–incommensurate transitions and quasiperiodic structures associated with the mismatch between the periodicities of the forcing and the critical mode. In Section 5 we will reformulate these results in terms of the mismatch in the periodicities of cortical activity

patterns and the underlying functional architecture of cortex. Note that the general form of the amplitude Eq. (4.10) can be derived using symmetry arguments [15]. For example, the first two terms on the right-hand side can be obtained by Fourier–Laplace transforming the dispersion relation (4.3) and rescaling. In the homogeneous case ($\gamma = 0$), the amplitude equation is equivariant with respect to the transformation $A \to A\,\mathrm{e}^{\mathrm{i}\phi}$, which reflects the translation invariance of the system. The lowest-order nonlinear term that has this symmetry is a cubic. The final term on the right-hand side of Eq. (4.10) reflects a discrete phase symmetry that persists when the inhomogeneity $D(\mathbf{r})$ satisfies the near-resonance condition (4.5). Note that symmetry arguments are not sufficient to determine the model-dependent coefficients $\alpha, \beta, \gamma, \omega$, which can only be calculated explicitly by carrying out some form of perturbation expansion. Given the nonlocal nature of the original evolution Eq. (2.10), it is worthwhile presenting the details of this calculation here. Moreover, the actual value of the coefficients is important. First, α determines the effective coherence length ξ_X of long-wavelength fluctuations according to $\xi_X = \sqrt{\alpha}/\varepsilon$; the validity of Eq. (4.10) requires that $\xi_X \ll L$, where L is the system size. Second, the sign of β determines whether or not the bifurcation is supercritical or subcritical. Third, all of the coefficients determine whether or not pinning occurs (see Section 5).

4.2. Case $\kappa = 0$

Setting $\kappa = 0$ in Eq. (4.4) and expanding to $\mathcal{O}(\varepsilon^3)$ leads to the following set of equations:

$$a_0 = \bar{W}_0 f(a_0) + h_0, \tag{4.11}$$

$$\mathcal{H}a_1 = 0, \tag{4.12}$$

$$\mathcal{H}a_2 = W * [g_2 a_1^2 + \mu_c \mathcal{Q}_1 a_1] \equiv b_2, \tag{4.13}$$

$$\mathcal{H}a_3 = -\frac{\partial a_1}{\partial T} + W * [a_1 + g_3 a_1^3 + 2g_2 a_1 a_2 + \mu_c \mathcal{Q}_2 a_1 + \mu_c \mathcal{Q}_1 a_2 + 2g_2 a_1 \mathcal{Q}_1 a_1], \equiv b_3. \tag{4.14}$$

Here $*$ denotes convolution with respect to the fast spatial variables

$$W * a(x) = \int W(x - x') a(x')\,\mathrm{d}x'. \tag{4.15}$$

$\mathcal{H}$ is the linear operator

$$\mathcal{H}a = a - \mu_c W * a, \tag{4.16}$$

and

$$W * \mathcal{Q}_n a(x, X, T) = \frac{1}{n!} \int W(x - x')(x' - x)^n \frac{\partial^n a(x', X, T)}{\partial X^n} \mathrm{d}x'. \tag{4.17}$$

The $\mathcal{O}(1)$ equation determines the fixed point a_0 whereas the $\mathcal{O}(\epsilon)$ equation has the critical roll solution (4.9).

A dynamical equation for the complex amplitude $A(X, T)$ can be derived by considering solvability conditions for the inhomogeneous linear Eqs. (4.13) and (4.14), which have the form $\mathcal{L}a_n = b_n$ for $n = 2, 3$. Since the linear operator $\mathcal{H}$ has a one-dimensional kernel, namely the critical mode (4.9), each inhomogeneous equation only has a solution if b_n is orthogonal to the kernel of $\mathcal{H}^\dagger$, the operator adjoint to $\mathcal{H}$. If we define the inner product of two periodic functions $U(x)$, $V(x)$ according to

$$\langle V|U\rangle = \frac{1}{L} \int_0^L V^*(x) U(x)\,\mathrm{d}x, \tag{4.18}$$

where L is the system size, then $\mathcal{H}$ is actually self-adjoint. Hence, setting $V = \mathrm{e}^{\mathrm{i}k_c x}$ we obtain the solvability conditions

$$\langle V|b_n\rangle = 0, \tag{4.19}$$

together with their complex conjugates. (Recall that under periodic boundary conditions $k_c = 2\pi n_c/L$ for some integer n_c so that V is an L-periodic function.)

In order to simplify the calculation we take $g_2 = 0$, since this does not alter the structure of the resulting amplitude equation. The $\mathcal{O}(\varepsilon^2)$ Eq. (4.13) then becomes $\mathcal{H}a_2 = \mu_c W * \mathcal{Q}_1 a_1$, where

$$W * \mathcal{Q}_1 a_1(x, X, T) = \int W(x - x')(x' - x)\frac{\partial A(X, T)}{\partial X}\,\mathrm{e}^{\mathrm{i}k_c x'}\mathrm{d}x' + \text{c.c.} = -\mathrm{i}\frac{\partial A(X, T)}{\partial X}\,\frac{\partial \tilde{W}(k)}{\partial k}\bigg|_{k=k_c} = 0, \tag{4.20}$$

since $\tilde{W}'(k_c) = 0$. Hence, the $\mathcal{O}(\varepsilon^2)$ Eq. (4.13) reduces to $\mathcal{H}a_2 = 0$ with solution $a_2 \sim a_1$. [In the case $g_2 \neq 0$ there are also zeroth and second-order harmonic contributions to a_2.] We are thus free to set $a_2 = 0$ so that the $\mathcal{O}(\varepsilon^3)$ solvability condition is

$$\left\langle V\middle|\frac{\partial a_1}{\partial T}\right\rangle = \langle V|W * [a_1 + g_3 a_1^3 + \mu_c \mathcal{Q}_2 a_1]\rangle. \tag{4.21}$$

The term $W * \mathcal{Q}_2 a_1$ can be determined along similar lines to $W * \mathcal{Q}_1 a_1$ and we find that

$$\begin{aligned} W * \mathcal{Q}_2 a_1(x, X, T) &= \frac{1}{2}\int W(x - x')(x' - x)^2\frac{\partial^2 A(X, T)}{\partial X^2}\,\mathrm{e}^{\mathrm{i}k_c x'}\mathrm{d}x' + \text{c.c.} \\ &= -\frac{1}{2}\,\mathrm{e}^{\mathrm{i}k_c x}\frac{\partial^2 A(X, T)}{\partial X^2}\,\frac{\partial^2 \tilde{W}}{\partial k^2}\bigg|_{k=k_c} + \text{c.c.} \end{aligned} \tag{4.22}$$

The various inner products in Eq. (4.21) can now be evaluated straightforwardly. For example

$$\langle V|W * a_1^3\rangle = \frac{1}{L}\int_0^L \mathrm{e}^{-\mathrm{i}k_c x}\tilde{W}(k_c)\left[A\,\mathrm{e}^{\mathrm{i}k_c x} + A^*\,\mathrm{e}^{-\mathrm{i}k_c x}\right]^3 \mathrm{d}x = 3\tilde{W}(k_c)A|A|^2. \tag{4.23}$$

Collecting together all our results then leads to the Ginzburg–Landau amplitude Eq. (4.10) with coefficients

$$\omega = \tilde{W}(k_c), \qquad \alpha = -\tfrac{1}{2}\mu_c\tilde{W}''(k_c), \qquad \beta = -3g_3\tilde{W}(k_c), \qquad \gamma = 0. \tag{4.24}$$

4.3. Case $\kappa = \mathcal{O}(\varepsilon^2)$

Setting $\kappa = \varepsilon^2\kappa_0$ in Eq. (4.4) and expanding to $\mathcal{O}(\varepsilon^3)$ generates additional terms in Eqs. (4.13) and (4.14):

$$\mathcal{H}a_2 = b_2 + \kappa_0 D\bar{J} f(a_0), \tag{4.25}$$

$$\mathcal{H}a_3 = b_3 + \kappa_0\mu_c DJ * a_1, \tag{4.26}$$

where $\bar{J} = \int J(x)\,\mathrm{d}x$ and D is given by Eq. (4.6). Assuming for simplicity that $g_2 = 0$, we find that $b_2 = 0$ so that Eq. (4.25) becomes $\mathcal{H}a_2 = \kappa_0 DJ_0 f(a_0)$, which has the particular solution

$$a_2(x, X, T) = \frac{\kappa_0\bar{J} f(a_0)}{1 - \mu_c\tilde{W}(nk_c/m)}D(x, X). \tag{4.27}$$

Note that we are free to set the complementary part of a_2 to be zero such that a_2 does not contribute to the $\mathcal{O}(\varepsilon^3)$ solvability condition. The latter reduces to Eq. (4.21) with an additional term arising from the horizontal interactions:

$$\left\langle V\Big|\frac{\partial a_1}{\partial T}\right\rangle = \langle V|W * [a_1 + g_3 a_1^3 + \mu_c \mathcal{Q}_2 a_1]\rangle + \kappa_0 \mu_c \langle V|DJ * a_1\rangle. \tag{4.28}$$

The final inner product on the right-hand side can be evaluated as follows:

$$\begin{aligned}\langle V|DJ * a_1\rangle &= \frac{1}{L}\int_0^L \mathrm{e}^{-\mathrm{i}k_c x}[\mathrm{e}^{\mathrm{i}nk_c x/m}\,\mathrm{e}^{\mathrm{i}nqX/m} + \text{c.c.}]\tilde{J}(k_c)[A(X,T)\,\mathrm{e}^{\mathrm{i}k_c x} + \text{c.c.}]\,\mathrm{d}x \\ &= \delta_{2m,n}\,\mathrm{e}^{\mathrm{i}2qX}\tilde{J}(k_c)A^*(X,T).\end{aligned} \tag{4.29}$$

Hence, when $\kappa = \mathcal{O}(\varepsilon^2)$ and the near-resonance condition (4.5) holds with $n = 2m$, the resulting amplitude equation is given by (4.10) for $n = 2$, with the coefficients ω, α, β satisfying Eq. (4.24) and

$$\gamma = \kappa_0 \mu_c \tilde{J}(k_c). \tag{4.30}$$

We conclude that if the periodicity of the horizontal connections is approximately half the wavelength of the roll pattern at the primary instability, $d \approx \pi/k_c$, then the corresponding synaptic interactions can couple to the cubic order amplitude equation.

4.4. Case $\kappa = \mathcal{O}(\varepsilon)$

Setting $\kappa = \varepsilon\kappa_0$ in Eq. (4.4) and expanding to $\mathcal{O}(\varepsilon^3)$ generates additional terms in Eqs. (4.12)–(4.14):

$$\mathcal{H}a_1 = \kappa_0 D\bar{J} f(a_0), \qquad \mathcal{H}a_2 = b_2 + \kappa_0 \mu_c DJ * a_1, \tag{4.31}$$

$$\mathcal{H}a_3 = b_3 + \kappa_0 DJ * [\mu_c a_2 + \mu_c \mathcal{Q}_1 a_1 + g_2 a_1^2]. \tag{4.32}$$

We take D to be given by Eq. (4.6) with p satisfying the near-resonance condition (4.5). The solution of the first-order Eq. (4.31) now consists of complementary and particular parts. If the complementary solution is taken to be a roll pattern along the x-axis then

$$a_1(x,X,T) = A(X,T)\,\mathrm{e}^{\mathrm{i}k_c x} + \Gamma\,\mathrm{e}^{\mathrm{i}nk_c x/m}\,\mathrm{e}^{\mathrm{i}nqX/m} + \text{c.c.}, \tag{4.33}$$

where

$$\Gamma = \frac{\kappa_0 \bar{J} f(a_0)}{1 - \mu_c \tilde{W}(nk_c/m)}. \tag{4.34}$$

Setting $g_2 = 0$ and substituting Eq. (4.33) into (4.32), we find that the particular solution for a_2 is

$$\begin{aligned}a_2(x,X,T) = \mathcal{A}_0 &+ \mathcal{A}_1\,\mathrm{e}^{\mathrm{i}(n/m)k_c x}\,\mathrm{e}^{\mathrm{i}(n/m)qX} + \mathcal{A}_2\,\mathrm{e}^{\mathrm{i}(2n/m)k_c x}\,\mathrm{e}^{\mathrm{i}(2n/m)qX} \\ &+ [\mathcal{A}_+\,\mathrm{e}^{\mathrm{i}(1+n/m)k_c x}\,\mathrm{e}^{\mathrm{i}(n/m)qX} + \mathcal{A}_-\,\mathrm{e}^{\mathrm{i}(1-n/m)k_c x}\,\mathrm{e}^{-\mathrm{i}(n/m)qX}]A(X,T) + \text{c.c.},\end{aligned} \tag{4.35}$$

where

$$\mathcal{A}_0 = \frac{\kappa_0 \mu_c \Gamma \tilde{J}(nk_c/m)}{1 - \mu_c \tilde{W}(0)}, \qquad \mathcal{A}_\pm = \frac{\kappa_0 \mu_c \tilde{J}(k_c)}{1 - \mu_c \tilde{W}(nk_c/m \pm k_c)}, \tag{4.36}$$

$$\mathcal{A}_1 = \frac{\mu_c \Gamma \tilde{W}'(nk_c/m)}{1 - \mu_c \tilde{W}(nk_c/m)}\frac{nq}{m}, \qquad \mathcal{A}_2 = \frac{\kappa_0 \mu_c \Gamma \tilde{J}(nk_c/m)}{1 - \mu_c \tilde{W}(2nk_c/m)}. \tag{4.37}$$

The associated solvability condition requires: (i) $\tilde{J}(k_c/2) = 0$ when $m = 2n$; (ii) $\tilde{J}(k_c) = 0$ when $n = 2m$ (at least to the given order of ε). We choose the complementary part of a_2 to be zero.

The $\mathcal{O}(\varepsilon^3)$ solvability condition can be written as

$$\left\langle V \middle| \frac{\partial a_1}{\partial T} \right\rangle = \langle V|W * [a_1 + g_3 a_1^3 + \mu_c \mathcal{Q}_2 a_1]\rangle + \mu_c \langle V|W * \mathcal{Q}_1 a_2\rangle + \kappa_0 \mu_c \langle V|DJ * [\mathcal{Q}_1 a_1 + a_2]\rangle. \tag{4.38}$$

Eq. (4.35) together with the $\mathcal{O}(\varepsilon^2)$ solvability conditions imply that $\langle V|W * \mathcal{Q}_1 a_2\rangle = 0$. Eq. (4.17), (4.22) and (4.23) imply that

$$W * \mathcal{Q}_2 a_1 = -\frac{1}{2}\, \mathrm{e}^{\mathrm{i}k_c x} \tilde{W}''(k_c) \frac{\partial^2}{\partial X^2} A(X,T) + \text{c.c.} + \Gamma W * \mathcal{Q}_2 D \tag{4.39}$$

with

$$W * \mathcal{Q}_2 D = \frac{1}{2} \left(\frac{nq}{m}\right)^2 \mathrm{e}^{\mathrm{i}nk_c x/m}\, \mathrm{e}^{\mathrm{i}nqX/m}\, \tilde{W}''(nk_c/m) + \text{c.c.} \tag{4.40}$$

Thus

$$\langle V|W * \mathcal{Q}_2 a_1\rangle = -\frac{1}{2} \tilde{W}''(k_c) \frac{\partial^2}{\partial X^2} A(X,T). \tag{4.41}$$

Expanding a_1^3 using Eq. (4.33) yields

$$\langle V|W * a_1^3\rangle = g_3 \tilde{W}(k_c)(3A|A|^2 + 6|\Gamma|^2 A + 3\delta_{n,3m} A^{*2} \Gamma\, \mathrm{e}^{3\mathrm{i}qX} + \Gamma^3 \delta_{3n,m}\, \mathrm{e}^{\mathrm{i}qX}). \tag{4.42}$$

Eqs. (4.17), (4.22) and (4.33) show that

$$J * \mathcal{Q}_1 a_1 = -\mathrm{i} \frac{\partial A^*}{\partial X}\, \mathrm{e}^{\mathrm{i}k_c x} \tilde{J}'(k_c) + \frac{nq\Gamma}{m}\, \mathrm{e}^{\mathrm{i}nk_c x/m}\, \mathrm{e}^{\mathrm{i}nqX/m}\, \tilde{J}'(nk_c/m) + \text{c.c.}, \tag{4.43}$$

and hence (for $n \neq 2m$, $m \neq 2n$)

$$\langle V|DJ * \mathcal{Q}_1 a_1\rangle = 0. \tag{4.44}$$

Finally, Eq. (4.35) implies that

$$\langle V|DJ * a_2\rangle = \mathcal{A}_2 \tilde{J}(2k_c/3)\, \mathrm{e}^{\mathrm{i}qX} \delta_{3n,m} + [\mathcal{A}_+ \tilde{J}([1 + n/m]k_c) + \mathcal{A}_- \tilde{J}([1 - n/m]k_c)]A. \tag{4.45}$$

Combining all of the above results, we deduce that when $\kappa = \mathcal{O}(\varepsilon)$ and the near-resonance condition (4.5) holds with $n = 3m$, the resulting amplitude equation is given by (4.10) for $n = 3$, with the coefficients α, β satisfying Eq. (4.24), and

$$\omega = \tilde{W}(k_c)(1 + 6g_3|\Gamma|^2) + \kappa_0 \mu_c [\mathcal{A}_+ \tilde{J}([1 + n/m]k_c) + \mathcal{A}_- \tilde{J}([1 - n/m]k_c)], \qquad \gamma = 3g_3 \tilde{W}(k_c)\Gamma. \tag{4.46}$$

Similarly, if $m = 3n$ then we obtain Eq. (4.10) for $n = 1$ with γ given by

$$\gamma = \kappa_0 \mu_c \mathcal{A}_2 \tilde{J}(\tfrac{2}{3}k_c). \tag{4.47}$$

5. Commensurate–incommensurate transitions in cortex

The amplitude Eq. (4.10) was previously derived using symmetry arguments within the context of a convective fluid system with spatially periodic forcing [15]. By studying solutions of this equation, it was shown how competition

between the periodicities of the external forcing and the critical modes of a primary pattern forming instability could lead to commensurate–incommensurate transitions mediated by soliton-like phase disturbances [15,29]. In this section we review the basic theory of commensurate–incommensurate transitions, and discuss its implications for cortical pattern formation.

First, it is useful to rewrite Eq. (4.10) in the rescaled form

$$\frac{\partial A}{\partial T} = \omega A + \frac{\partial^2 A}{\partial X^2} - |A|^2 A + \gamma A^{*n-1}\,\mathrm{e}^{\mathrm{i}nqX}, \tag{5.1}$$

where $X \to X/\sqrt{\alpha}$, $A \to \sqrt{\beta}A$, $q \to \sqrt{\alpha}q$ and $\gamma \to \gamma\beta^{(2-n)/2}$. Setting $A = R\,\mathrm{e}^{\mathrm{i}\Theta}$, we obtain the pair of equations

$$\frac{\partial R}{\partial T} = \omega R - R^3 + \frac{\partial^2 R}{\partial X^2} - \left(\frac{\partial \Theta}{\partial X}\right)^2 R + \gamma R^{n-1}\cos[n(\Theta - qX)], \tag{5.2}$$

and

$$R\frac{\partial \Theta}{\partial T} = R\frac{\partial^2 \Theta}{\partial X^2} + 2\frac{\partial R}{\partial X}\frac{\partial \Theta}{\partial X} - \gamma R^{n-1}\sin[n(\Theta - qX)]. \tag{5.3}$$

These have stationary solutions of the form

$$\Theta = \Theta_0(X) = qX + \frac{p\pi}{n}, \qquad R = R_0 \tag{5.4}$$

with R_0 satisfying

$$\omega - q^2 - R_0^2 + \gamma(-1)^p R_0^{n-2} = 0 \tag{5.5}$$

for integers p. These represent uniform roll patterns corresponding to the unstable band of modes close to the primary instability.

We investigate the stability of the stationary solutions by substituting

$$R = R_0 + r(X,T), \qquad \Theta = \Theta_0(X) + \phi(X,T) \tag{5.6}$$

into Eqs. (5.2) and (5.3) and expanding to first-order in ϕ, r. This yields the pair of linear equations

$$\frac{\partial r}{\partial T} = -\Omega_r r + \frac{\partial^2 r}{\partial X^2} - 2R_0 q\frac{\partial \phi}{\partial X}, \tag{5.7}$$

and

$$\frac{\partial \phi}{\partial T} = -\Omega_\phi \phi + \frac{\partial^2 \phi}{\partial X^2} + \frac{2q}{R_0}\frac{\partial r}{\partial X} \tag{5.8}$$

with

$$\Omega_r = -[\omega - q^2 - 3R_0^2 + (-1)^p(n-1)\gamma R_0^{n-2}], \tag{5.9}$$

and

$$\Omega_\phi = (-1)^p \gamma n R_0^{n-2}. \tag{5.10}$$

It immediately follows from Eqs. (5.8) and (5.10) that the stationary solutions for odd p are unstable with respect to phase perturbations, since $\Omega_\phi < 0$. Now suppose $\Omega_r \gg \Omega_\phi > 0$ for even p, so that the amplitude perturbations r adiabatically follow the phase fluctuations ϕ. We can then make the approximation

$$\Omega_r r = -2R_0 q\frac{\partial \phi}{\partial X}, \tag{5.11}$$

which leads to the following phase equation for $\Phi = \Theta - qX$ [15]:

$$\frac{\partial \Phi}{\partial T} = \Delta \frac{\partial^2 \Phi}{\partial X^2} - \mathcal{K} \sin(n\Phi) = -\frac{\delta \mathcal{V}}{\delta \Phi}, \tag{5.12}$$

where

$$\Delta = 1 - \frac{4q^2}{\Omega_r}, \qquad \mathcal{K} = \gamma R_0^{n-2}, \tag{5.13}$$

and

$$\mathcal{V} = \int \left[\frac{\Delta}{2} (\partial_X \Phi + q)^2 - \frac{\mathcal{K}}{n} \cos(n\Phi) \right] \mathrm{d}x. \tag{5.14}$$

Eq. (5.12) is identical to the sine-Gordon equation used to describe commensurate–incommensurate transitions in solids, for which structural configurations correspond to minima of the effective potential $\mathcal{V}$ [4]. For the purposes of the current discussion, we will neglect the q-dependence of Δ and assume that it is fixed. We note, however, that it is possible for Δ to become negative as q increases, leading to the analog of an Eckhaus instability (see [17,46] for more details). From well known properties of the sine-Gordon equation, the following results then hold:

1. There exists a critical value q_0 defined by

$$q_0^2 = \frac{16\mathcal{K}}{n\pi^2 \Delta}, \tag{5.15}$$

   such that when $q < q_0$ the minimum of the potential $\mathcal{V}$ corresponds to a locked state $\Phi = 2\pi p/n$. Recall that q is a measure of the mismatch between the spatial frequencies of the primary roll pattern and the cortical lattice as specified by the near-resonance condition (4.5). It follows that when this mismatch is sufficiently small, the activity pattern is pinned to the lattice with $a(x) \sim \cos(2\pi m x/nd)$. In the particular case $n = 2$ this corresponds to the even mode shown in Fig. 9. Thus our nonlinear analysis has established that the even (odd) mode is stable (unstable) to phase fluctuations and that the pinning of the stable mode persists over a range of values of the pattern wavenumber.
2. When the mismatch $q > q_0$, the minimum of the potential $\mathcal{V}$ occurs for soliton-like solutions of the sine-Gordon equation. A single soliton solution is of the form

$$\Phi(X) = \frac{4}{n} \tan^{-1} \exp\left(\sqrt{n\mathcal{K}} X\right). \tag{5.16}$$

   This describes a kink centered at $X = 0$ that separates two regions of the roll pattern each of which is commensurate with the cortical lattice, one with phase $\Phi = 0$ and one with phase $\Phi = 2\pi/n$. More generally, the solutions are regularly spaced solitons as illustrated in Fig. 11. The average phase-shift of the roll pattern per unit length is then

$$\rho = \frac{2\pi}{nl}, \tag{5.17}$$

   where l is the separation between neighboring kinks. Equivalently, ρ is a measure of the soliton density. It can be shown that

$$\frac{\rho}{q} = \frac{4}{\pi^2} K(\eta) E(\eta), \tag{5.18}$$

   where K and E are complete elliptic integrals of first and second kind, and η satisfies the equation

$$\frac{q_0}{q} = \frac{\pi \eta}{2E(\eta)}. \tag{5.19}$$

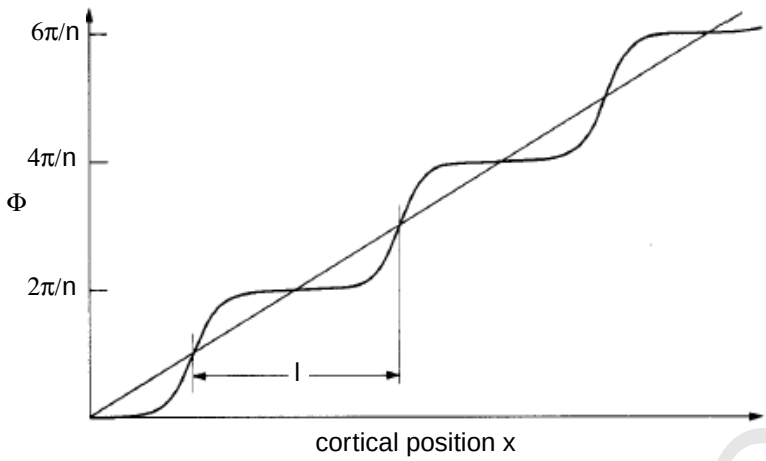

Fig. 11. Multi-soliton solution to the sine-Gordon equation that describes regions of the roll pattern that are commensurate with the cortical lattice separated by domain walls of mean separation l.

An asymptotic analysis of these equations establishes that $\rho \sim \log(q - q_0)$ for $q \to q_0$ [4]. We conclude that if the mismatch between the periodicities of the activity pattern and cortical lattice is increased such that $q > q_0$, then there is a commensurate–incommensurate transition to a state in which the activity pattern is no longer pinned to the lattice due to the formation of soliton-like phase defects.

6. Discussion

In this paper we have shown how periodic inhomogeneities in the distribution of long-range horizontal connections can lock spontaneously formed activity patterns in visual cortex to an underlying lattice of periodic feature maps. There are a number of interesting issues that arise from this: (i) We have focused on the distribution of CO blobs in visual cortex, since this is one candidate structure for breaking the translation symmetry of cortex. However, the same methods could also be applied to other lattice-like structures such as the distribution of orientation singularities. The CO blobs appear to coincide with about half the singularities, namely those associated with low spatial frequencies [26]. (ii) We have assumed for simplicity that the cortex has a regular crystalline-like structure. A more realistic model would need to take into account the effects of topological and substitutional disorder within this structure. (iii) Our mechanism for the pinning of cortical patterns assumes that there exist long-wavelength phase fluctuations as described by solutions of the amplitude Eq. (4.10). The validity of this equation requires that the size of cortex is sufficiently large to support such fluctuations, with the latter having an effective coherence length of $\sqrt{\alpha}/\varepsilon$. Otherwise, boundary effects are likely to play an important role.

It is important to emphasize that the cortical activity patterns discussed in this paper do not generate the underlying feature maps, rather they occur in a neural medium that has a set of feature maps hardwired into it. For example, if $a(\mathbf{r})$ is the activity at position $\mathbf{r}$ in the cortical sheet and $\mathcal{F}(\mathbf{r})$ represents the corresponding feature preferences of the neurons at $\mathbf{r}$, then the level of activity codes for these particular features. The feature maps $\mathcal{F}(\mathbf{r})$ are themselves determined by the feedforward projections to the cortex from the LGN. An interesting question is how the feedforward connections develop in the immature cortex in order to form the feature maps in the first place? Consider as an example the development of ocular dominance columns. Activity-based developmental models typically involve some Hebbian-like competitive mechanism for the modification of left/right eye feedforward connections under

the assumption that the intracortical connections are fixed [43]. Intracortical interactions consisting of short-range excitation and longer-range inhibition mediate a pattern forming instability with respect to the feedforward synaptic weights, which can lead to the formation of alternating stripes of left and right eye dominated columns [42]. Interestingly, the intracortical interactions are usually taken to be homogeneous, so there is no intrinsic mechanism for aligning the centers of the columns with the CO blobs, as is observed in macaques, for example [36]. This latter property is clearly seen in the optical imaging data of Fig. 1, and is further illustrated schematically in Fig. 4. We hypothesize that such an alignment may be due to a pinning mechanism analogous to the one considered in this paper. In order for pinning of the feedforward connections to occur, there must exist some source of spatial inhomogeneity in the lateral interactions that correlates with the CO blobs early in development. There is growing experimental evidence to support such a claim. For example, the spacing and packing arrangement of CO blobs is not affected by strabismus in macaques [33] nor by early visual deprivation in cats [34]. The lack of influence of visual experience on their development suggests that the CO blobs may reflect an innate columnar organization within the immature cortex that follows the arrangement of intrinsic chemical markers. A number of anatomical markers are arranged in a patchy fashion during development, including the NMDA receptor, which plays a key role in experience-dependent plasticity [45]. These markers could mediate the lateral interactions early in development as well as provide a substrate for the formation of the patchy horizontal connections [13,39,14].

Acknowledgements

The author would like to thank Professor Jack Cowan (University of Chicago) for many helpful discussions. This work was supported by NSF grant DMS-0209824.

Appendix A

In this appendix we show that our prescription for introducing a slow spatial scale into the nonlocal integro-differential Eq. (4.4) is consistent with the corresponding scaling used in PDEs. Since the treatment of time is identical in both cases, we focus on the following time-independent integral equation

$$a(x) = \int_{-\infty}^{\infty} W(x - x') f(a(x'))\, \mathrm{d}x'. \tag{A.1}$$

In the case of an exponential weight distribution, $W(x) = \mathrm{e}^{-|x|}/2$, the convolution over space can be eliminated using the identity

$$(1 - \partial_{xx}) W(x - x') = \delta(x - x'), \tag{A.2}$$

where $\partial_{xx} = \partial^2/\partial x^2$. That is, Eq. (A.1) is equivalent to the differential equation

$$(1 - \partial_{xx}) a(x) = f(a(x)). \tag{A.3}$$

Let us now apply the operator $1 - \partial_{xx}$ to the corresponding multiple scale version of Eq. (A.1)

$$a(x, X) = \int_{-\infty}^{\infty} W(x - x') f(a(x', X + \varepsilon(x' - x)))\, \mathrm{d}x', \tag{A.4}$$

which we can rewrite as

$$a(x, \hat{X} + \varepsilon x) = \int_{-\infty}^{\infty} W(x - x') f(a(x', \hat{X} + \varepsilon x'))\, \mathrm{d}x', \tag{A.5}$$

under the change of coordinates $\hat{X} = X - \varepsilon x$. This gives

$$(1 - \partial_{xx})a(x, \hat{X} + \varepsilon x) = f(a(x, \hat{X} + \varepsilon x)), \tag{A.6}$$

or

$$(1 - [\partial_x + \varepsilon \partial_X]^2)a(x, X) = f(a(x, X)). \tag{A.7}$$

Eq. (A.7) is the expected multiple scale version of the differential Eq. (A.3).

References

[1] N.W. Ashcroft, N.D. Mermin, Solid State Physics, Saunders, London, 1976.
[2] K.D. Alloway, J. Crist, J.J. Mutic, S.A. Roy, Corticostriatal projections from rat barrel cortex have an anisotropic organization that correlates with vibrissal whisking behavior, J. Neurosci. 19 (1999) 10908–10922.
[3] A. Angelucci, J.B. Levitt, E.J.S. Walton, J.-M. Hupe, J. Bullier, J.S. Lund, Circuits for local and global signal integration in primary visual cortex, J. Neurosci. 22 (2002) 8633–8646.
[4] P. Bak, Commensurate phases, incommensurate phases and the devil's staircase, Rep. Prog. Phys. 45 (1982) 587–629.
[5] G.G. Blasdel, Orientation selectivity, preference, and continuity in monkey striate cortex, J. Neurosci. 12 (1992) 3139–3161.
[6] G.G. Blasdel, D. Campbell, Orientation selectivity, preference, and continuity in monkey striate cortex, J. Neurosci. 21 (2001) 8286–8301.
[7] W.H. Bosking, Y. Zhang, B. Schofield, D. Fitzpatrick, Orientation selectivity and the arrangement of horizontal connections in tree shrew striate cortex, J. Neurosci. 17 (1997) 2112–2127.
[8] P.C. Bressloff, J.D. Cowan, M. Golubitsky, P.J. Thomas, M. Wiener, Geometric visual hallucinations, Euclidean symmetry and the functional architecture of striate cortex, Phil. Trans. Roy. Soc. Lond. B 356 (2001) 299–330.
[9] P.C. Bressloff, J.D. Cowan, M. Golubitsky, P.J. Thomas, Scalar and pseudoscalar bifurcations: pattern formation on the visual cortex, Nonlinearity 14 (2001) 739–775.
[10] P.C. Bressloff, Bloch waves, periodic feature maps and cortical pattern formation, Phys. Rev. Lett. 89 (2002) 088101.
[11] P.C. Bressloff, J.D. Cowan, The visual cortex as a crystal, Physica D (2002) 226–258.
[12] P.C. Bressloff, J.D. Cowan, Spontaneous pattern formation in primary visual cortex, in: S.J. Hogan, A. Champneys, B. Krauskopf (Eds.), Nonlinear Dynamics and Chaos: Where Do We Go From Here? Institute of Physics, Bristol, 2002.
[13] E.M. Calloway, L.C. Katz, Experience and refinement of clustered horizontal connections in cat striate cortex, J. Neurosci. 10 (1990) 1134–1154.
[14] C. Chiu, M. Weliky, Relationship of correlated spontaneous activity to functional ocular dominance columns in the developing visual cortex, Neuron 35 (2002) 1123–1134.
[15] P. Coullet, Commensurate–incommensurate transition in nonequilibrium systems, Phys. Rev. Lett. 56 (1986) 724–727.
[16] J.D. Cowan, Spontaneous symmetry breaking in large scale nervous activity, Int. J. Quant. Chem. 22 (1982) 1059–1082.
[17] M.C. Cross, A.C. Newell, Convection patterns in large aspect ration systems, Physica D 10 (1984) 299–328.
[18] M.C. Cross, P.C. Hohenberg, Pattern formation outside of equilibrium, Rev. Mod. Phys. 65 (1993) 851–1111.
[19] G.B. Ermentrout, J.D. Cowan, A mathematical theory of visual hallucination patterns, Biol. Cybernet. 34 (1979) 137–150.
[20] G.B. Ermentrout, J.D. Cowan, Secondary bifurcation in neuronal nets, SIAM J. Appl. Math. 39 (1980) 323–340.
[21] G.B. Ermentrout, Neural networks as spatial pattern forming systems, Rep. Prog. Phys. 61 (1998) 353–430.
[22] D. Fitzpatrick, Seeing beyond the receptive field in primary visual cortex, Curr. Opt. Neurobiol. 10 (2000) 438–443.
[23] C.D. Gilbert, T.N. Wiesel, Clustered intrinsic connections in cat visual cortex, J. Neurosci. 3 (1983) 1116–1133.
[24] J.D. Hirsch, C.D. Gilbert, Synaptic physiology of horizontal connections in the cat's visual cortex, J. Physiol. Lond. 160 (1992) 106–154.
[25] J.C. Horton, Cytochrome oxidase patches: a new cytoarchitectonic feature of monkey visual cortex, Phil. Trans. Roy. Soc. Lond. B 304 (1984) 199–253.
[26] S. LeVay, S.B. Nelson, Columnar organization of the visual cortex, in: A.G. Leventhal (Ed.), The Neural Basis of Visual Function, CRC Press, Boca Raton, 1991, pp. 266–315.
[27] J.B. Levitt, D.A. Lewis, T. Yoshioka, J.S. Lund, Topography of pyramidal neuron intrinsic connections in macaque prefrontal cortex, J. Comp. Neurol. 338 (1993) 360–376.
[28] M.S. Livingstone, D.H. Hubel, Specificity of intrinsic connections in primate primary visual cortex, J. Neurosci. 4 (1984) 2830–2835.
[29] M. Lowe, J.P. Gollub, Solitons and the commensurate–incommensurate transition in a convective nematic fluid, Phys. Rev. A 31 (1985) 3893–3896.
[30] J.S. Lund, A. Angelucci, P.C. Bressloff, Anatomical substrates for functional columns in macaque monkey primary visual cortex, Cereb. Cortex 12 (2003) 15–24.
[31] R. Malach, Y. Amir, M. Harel, A. Grinvald, Relationship between intrinsic connections and functional architecture revealed by optical imaging and in vivo targeted biocytin injections in primate striate cortex, Proc. Natl. Acad. Sci. 90 (1993) 10469–10473.

[32] D.S. Melchitzky, S.R. Sesack, M.L. Pucak, D.A. Lewis, Synaptic targets of pyramidal neurons providing intrinsic horizontal connections in monkey prefrontal cortex, J. Comp. Neurol. 390 (1998) 211–224.
[33] K.M. Murphy, D.G. Jones, S.B. Fenstemaker, V.D. Pegado, L. Kiorpes, J.A. Movshon, Spacing of cytochrome oxidase blobs in visual cortex of normal and strabismic monkeys, Cereb. Cortex 8 (1998) 237–244.
[34] K.M. Murphy, K.R. Duffy, D.G. Jones, D.E. Mitchell, Development of cytochrome oxidase blobs in visual cortex of normal and visually deprived cats, Cereb. Cortex 11 (2001) 237–244.
[35] A.C. Newell, J.A. Whitehead, Finite bandwidth, finite amplitude convection, J. Fluid Mech. 38 (1969) 279.
[36] K. Obermayer, G. Blasdel, Geometry of orientation and ocular dominance columns in monkey striate cortex, J. Neurosci. 13 (1993) 4114–4129.
[37] H.L. Read, J.A. Winer, C.E. Schreiner, Modular organization of intrinsic connections associated with spectral tuning in cat auditory cortex, Proc. Natl. Acad. Sci. USA 98 (2001) 8042–8047.
[38] K.S. Rockland, J.S. Lund, Intrinsic laminar lattice connections in primate visual cortex, J. Comp. Neurol. 216 (1983) 303–318.
[39] E.S. Ruthazer, M.P. Stryker, The role of activity in the development of long-range horizontal connections in area 17 of the ferret, J. Neurosci. 16 (1996) 7253–7269.
[40] L.A. Segel, Distant side-walls cause slow amplitude modulation of cellular convection, J. Fluid Mech. 38 (1969) 203.
[41] L.C. Sincich, J.C. Horton, Divided by cytochrome oxidase: a map of the projections from V1 to V2 in macaques, Science 295 (2002) 1734–1737.
[42] N.V. Swindale, A model for the formation of ocular dominance stripes, Proc. Roy. Soc. B 208 (1980) 243–264.
[43] N.V. Swindale, The development of topography in visual cortex: a review of models, Network 7 (1996) 161–247.
[44] L.J. Toth, S.C. Rao, D. Kim, S. Somers, M. Sur, Subthreshold facilitation and suppression in primary visual cortex revealed by intrinsic signal imaging, Proc. Natl. Acad. Sci. 93 (1996) 9869–9874.
[45] C. Trepel, K.R. Duffy, V.D. Pegado, K.M. Murphy, Patchy distribution of NMDAR1 subunit immunoreactivity in developing visual cortex, J. Neurosci. 18 (1998) 3404–3415.
[46] D. Walgraef, Spatio-Temporal Pattern Formation, Springer, Berlin, 1997.
[47] H. Werner, T. Richter, Circular stationary solutions in two-dimensional neural fields, Biol. Cybernet. 85 (2001) 211–217.
[48] H.R. Wilson, J.D. Cowan, A mathematical theory of the functional dynamics of cortical and thalamic nervous tissue, Kybernetik 13 (1973) 55–80.
[49] T. Yoshioka, G.G. Blasdel, J.B. Levitt, J.S. Lund, Relation between patterns of intrinsic lateral connectivity, ocular dominance, and cytochrome oxidase-reactive regions in macaque monkey striate cortex, Cereb. Cortex 6 (1996) 297–310.
[50] N.H. Yabuta, E.M. Callaway, Cytochrome-oxidase blobs and intrinsic horizontal connections of layer 2/3 pyramidal neurons in primate V1, Visual Neurosci. 15 (1998) 1007–1027.